MSc Thesis Civil Engineering & Management

Developing a data-driven hydrodynamic model of a marine environment

Using ship-based ADCP measurements in the North Sea

Wout Leemeijer

Graduation committee:
Dr. Ir. B.W. Borsje
Dr. Ir. J.H. Damveld
Dr. V. Kitsikoudis
Ir. T. Ligteringen

September 25, 2023

Water Engineering and Management (WEM)
Department of Civil Engineering & Management
Faculty of Engineering Technology
University of Twente

The Netherlands Hydrographic Service
Royal Netherlands Navy

UNIVERSITY OF TWENTE.

Koninklijke Marine

Preface

This document marks the end of my time as a student at the University of Twente. This thesis is the finalisation of my graduation project in Civil Engineering & Management for the specialisation River & Coastal Engineering, conducted internally, in collaboration with The Netherlands Hydrographic Service of the Royal Netherlands Navy.

I want to thank everyone who helped me with this project. First of all, I want to thank my daily supervisors Johan and Vasilis. Our weekly meetings, after we discussed the latest football news for some time, always helped me to get inspiration on how to continue with the project, to get feedback on what I had done so far, and you always helped me when my progress did not go as I would have wanted. Next, I want to thank Bas for being the head of my graduation committee and especially for thinking along and being flexible, when things were not going according to plan. Lastly, I want to thank Thijs for being involved as part of The Netherlands Hydrographic Service, for answering specific questions, for introducing me to other people who could help me and for inviting me to visit the ship in Den Helder that made the measurements for this project.

Furthermore, I have to thank some other people who helped me with this project. First of all, I want to thank Raymon van de Veen, Merte Peeters, Noortje ten Broeke, and all other people involved from the Royal Netherlands Navy for answering my questions, for making new measurements when the first set of measurements turned out to be not sufficient for this project and for welcoming me on the Zr.Ms. Snellius. Next, I want to thank Herman Huitema from Nortek for providing me with some background information about the way a DVL makes measurements and what possible mistakes might be present in my data set. Lastly, I want to thank Pauline Overes from the University of Twente and Deltares for running the Dutch Coastal Shelf Model so that I could use the results in my validation.

I hope you enjoy reading my master's thesis.

Summary

Hydrodynamic data is used as input data for many different models such as morphological models. The two main sources of flow velocity data that are currently used are buoys and coastal shelf models. Buoys have the disadvantage that they lack spatial resolution, and hence the spatial variation in the flow velocities is not taken into account. Coastal shelf models have the disadvantage that the models are calibrated on water levels, causing there to be an overestimation of 0.2 up to 0.6 m/s of the flow velocity predictions, while the accuracy of a hydrodynamic model should be within ± 0.2 m/s. A possible solution to both problems is making use of ship-based flow velocity measurements, made while the ship is sailing. These measurements vary both in space and time and therefore have a higher spatial resolution than buoy measurements. Furthermore, previous studies showed that the accuracy of these measurements is within 0.04 m/s and hence an improvement on coastal shelf models. The Netherlands Hydrographic Service of the Royal Netherlands Navy has mounted a Doppler Velocity Log (DVL) on one of their ships and has made such measurements. However, no methods are currently available to deal will flow velocity data that have both a temporal and spatial variation. In this study, the first steps are taken in the development of such a method.

A data set has been provided, containing four days of DVL measurements made near the Dutch coast. To make use of these measurements, first, the possible errors in the measurements are identified. First of all, the clock of the DVL and the software in the ship are not synchronized, causing the corrections for the heading and the pitch and roll to be applied at the wrong moment. This means that the moment the ship is turning should not be taken into account. Furthermore, the top layer of the water column is affected by the turbulence caused by the ship and the bottom layer by the side lobes of the DVL, meaning that both layers should not be taken into account. After leaving these data points out, obvious outliers in the data were filtered by looking at the deviation compared to the mean value of the measurements. Lastly, the water column is divided into two layers. This is done by looking at the velocity magnitude profile to identify the split point between the two layers. For both layers, the velocities are then averaged over the depth of each layer.

Using the pre-processed data the tidal signal is extracted using harmonic analysis for each depth layer. In the top layer the M2, M3, M4, 2MK5, M6 and M8 tide could be extracted, while in the bottom layer, only the M2 and 2MK5 could be extracted. The harmonic analysis makes a good estimation of the northward velocities, but the eastward velocities are twice as large as the measured velocities. The tidal signals are then used to make predictions about the tidal propagation in the model domain, which has been divided by a grid. For this two methods are developed. The STEP (Spatial-from-Temporal Estimated Phase) method relates the temporal phase difference between measurements to the spatial phase difference between measurements, while the WC (Wave Celerity) method is based the propagation on the wave celerity in the model domain.

The output of the STEP method showed that this method significantly overestimates the spatial phase difference with values of 20000° over a distance of 40 km. This overestimation is caused by not taking the sign of the temporal phase difference into account when averaging. For the WC method, this difference is only 40°, which is more realistic. Comparing the output of both methods with the Dutch Coastal Shelf Model (DCSM) shows that the output of the STEP method has a different phase and frequency compared to the DCSM leading to a cross-correlation of 0 and a Root-Mean-Squared Deviation (RMSD) of between 0.4 and 0.6 m/s. For the WC method, the phase and frequency of the output are more similar, leading to a high cross-correlation of 0.9 and an RMSD of 0.2 m/s. Comparing the two methods with measurements made with a buoy near IJmuiden did not help in validating the model, since the buoy only measures surface flow velocities and only the M8 tidal constituent could be extracted. This makes it hard to compare with the output of both models, since they can not predict surface flow velocities and include more tidal constituents.

All in all, this research shows the first steps in developing a method to deal with the spatial and temporal variation in ship-based DVL measurements. Since a ship-based DVL is able to make highly accurate flow velocity measurements, this can be used to improve hydrodynamic predictions, while also having a higher spatial resolution. However, before these methods can be applied they need to be improved and extended. For the STEP method to work the estimation of the spatial phase difference needs to be improved. On the other hand, the WC method shows promising results but only includes the tidal components of the flow. Finally, recommendations are made on how to continue this research. This includes synchronizing the DVL with the software on the ship and making measurements over a longer period, to improve the quality of the data, saving a part of the data set as a validation set and including more physical processes in the model.

Contents

Preface **2**

Summary **3**

1 Introduction **5**
1.1 Research Gap . . . 6
1.2 Research Objective . . . 6
1.3 Structure of the report . . . 7

2 Theoretical Background **7**
2.1 Doppler Velocity Log (DVL) . . . 7
2.2 Tidal Signal Analysis . . . 8

3 Data **9**
3.1 Description . . . 9
3.2 Pre-Processing . . . 11
3.2.1 Errors in the Measurements . . . 11
3.2.2 Time Log Difference . . . 11
3.2.3 Outliers . . . 11
3.3 Multilayer Depth Model . . . 13

4 Methods **16**
4.1 Harmonic Analysis . . . 16
4.2 Grid . . . 17
4.3 Tidal Propagation . . . 18
4.3.1 Spatial-from-Temporal Estimated Phase (STEP) Method . . . 19
4.3.2 Wave Celerity (WC) Method . . . 21
4.4 Validation Techniques . . . 22
4.4.1 Tidal Ellipse Verification . . . 22
4.4.2 Other Velocity Data Sources . . . 22

5 Results **23**
5.1 Tidal Signal . . . 23
5.2 Model Output . . . 25
5.2.1 STEP method . . . 25
5.2.2 WC method . . . 29

6 Validation **35**
6.1 Tidal Ellipse Parameter Verification . . . 35
6.2 Comparison with Other Data Sources . . . 36
6.2.1 Dutch Coastal Shelf Model . . . 36
6.2.2 Buoy data . . . 39

7 Discussion **41**

8 Conclusion **44**

9 Recommendations **45**
9.1 Quality of the Data . . . 45
9.2 Model Development . . . 45

A Appendix **A1**
A.1 Filtering Results . . . A1
A.2 Harmonic Analysis Output . . . A2
A.3 Harmonic Analysis Buoy . . . A2

1 Introduction

Hydrodynamic models can be used to simulate hydrodynamic scenarios in a marine environment. These models have many different applications. For example, ensembles of hydrodynamic models are used to make more accurate predictions about the effect of different scenarios of sea level rise in estuaries. Furthermore, hydrodynamic models are being used to reproduce changes from the past and to give possible physical explanations for these changes (Iglesias et al., 2022). Another application of these models is as input for morphological models. For example, the output of hydrodynamic models is used as input of morphological models to get insight into sand wave dynamics (e.g. Overes et al., 2023). In coastal shelf seas, various rhythmic bedforms occur, such as sand waves (Dyer and Huntley, 1999). Bedforms migrate over time, affecting the sea bed, which is largely caused by hydrodynamic factors near the sea bed (Li et al., 2021). The migration of these bedforms is especially relevant in intensively used coastal shelf seas, such as the North Sea, since this can affect navigation and the placement of wind farms. Furthermore, it can lead to exposure of cables, pipelines, or other objects on the sea floor (Games and Gordon, 2014).

To obtain accurate predictions in morphological models, high-quality hydrodynamic input data is needed, especially near the seabed. To get this input data, different sources are available, such as buoy measurements (e.g. Plecha et al., 2012). Buoy measurements have the advantage that they will provide high-quality flow velocity measurements for a long period of time (Wilson and Siegel, 2008), while a buoy has the disadvantage that it makes measurements at a set location, while there is a large spatial variation in flow velocities in the sea, which is not included in these measurements (Howarth and Proctor, 1992). Another source is from coastal shelf models such as the Dutch Coastal Shelf Model (DCSM) developed by Deltares (Zijl et al., 2023). The DCSM is a 3D-hydrodynamic model of the Dutch Coastal Shelf, combining currents, water temperature, salinity and water levels. This model can be used to make both short-term and long-term predictions and is used for water and coastal management. The model makes use of a set grid and can be run as both a 2DH and a 3D model. To predict the tidal water levels and velocities the DCSM makes use of 39 tidal constituents. The DCSM has the advantage that it makes predictions for the flow velocity for the entire Dutch Coastal Shelf at a high spatial and temporal resolution. However, the DCSM has the disadvantage that it is calibrated and validated based on water levels causing a higher uncertainty in the predictions for flow velocities. A quantitative comparison of the predictions of the DCSM model for flow velocities showed that for different configurations of the model, the depth-averaged flow velocities in the model are overestimated by 2-3 cm/s up to 6-7 cm/s (Zijl et al., 2018). Furthermore, near the water surface and the sea bed, the magnitudes are even worse, since at these locations many more processes influence the flow velocities (Zijl et al., 2018). It is recommended for hydrodynamic models that the predicted current velocities are within ± 2 cm/s of the measured velocities in coastal shelf seas (Williams and Esteves, 2017). Hence, this shows that the flow velocity predictions of the DCSM are not within the desired accuracy. Consequently, the hydrodynamic input data is not always of high quality. Therefore, to be able to get reliable predictions when using hydrodynamic data, the quality of this data should improve.

A possible solution is the use of hydrodynamic measurements made by The Netherlands Hydrographic Service of the Royal Netherlands Navy. They equipped one of their vessels with a Doppler Velocity Log (DVL). A DVL can be used in the same way as an Acoustic Doppler Current Profiler (ADCP), which is a widely used acoustic device for velocity and turbulence measurements (Nortek, 2023c). For example, a study by Fong and Jones (2006) shows a DVL used for making velocity measurements on an autonomous underwater vehicle. A DVL measures the velocity profile over the water column at a certain location by analysing the reflection of emitted sound pulses on the moving particles in the water column while assuming that the particles move at the same speed as the water flow (Horstman et al., 2011). DVL measurements will yield the flow velocity and flow direction for different water depths (Pandian et al., 2010). This can be used as an input for hydrodynamic and, eventually, morphological models. The Netherlands Hydrographic Service has made hydrodynamic measurements while sailing during multiple different periods near the Dutch coast using this ship-based DVL. This overcomes the lack of spatial information that the buoy has and can also improve the accuracy of the flow velocity data compared to the DCSM model. Hence, these measurements can possibly be used as a new source of input data for hydrodynamic and morphological models. Since The Netherlands Hydrographic Service makes measurements in all areas of the Dutch Coastal Shelf once in a while, the ship-based DVL measurements have the potential to lead to hydrodynamic input data for the whole Dutch Coastal Shelf.

Ship-based velocity measurements have been used before, for example, while sailing along a transect of a river, but mainly to get an indication of the uncertainty of those measurements (González-Castro and Muste, 2007). Another application of ship-based DVL measurements is as verification of flow velocity measurements

of large-scale models and shows the need for high-quality, high-resolution data in coastal areas (Ribotti et al., 2019). However, this only provides measurements at certain locations in the study area and can therefore not be used as a prediction for the whole study area at one moment in time. Furthermore, ship-based DVL measurements have been used as hydrodynamic input data for morphological models modelling sand wave migration (Zhou et al., 2022). However, in this case, the ship was sailing along a transect above the sand wave crest and hence still leads to a small spatial coverage in the data. A study by Sheehan et al. (2018) shows that ship-based DVL measurements can have an accuracy of within ± 0.4 cm/s, which means that the accuracy of these measurements is high. Furthermore, as shown by de Vreeze (2020), ship-based DVL measurements can be used to estimate the tidal ellipse and hence give insight into the tidal velocities at those locations. Therefore, ship-based DVL measurements have the potential to improve the hydrodynamic input data.

However, all previous studies using ship-based DVL measurements either use the data as a validation source or as hydrodynamic input, but still only for a transect, resulting in a small spatial coverage. At the moment there is no approach available to go from ship-based DVL measurements, where each measurement has both a spatial and temporal difference for the complete study area, to a hydrodynamic model of that area, with velocities at multiple locations for each time step. Having such an approach can increase the resolution of the available hydrodynamic flow velocity data while reducing the errors that exist in other models predicting flow velocities. This means that a method should be developed to predict the flow velocities at every location in the grid cell, which is based on the spatially and temporally distributed DVL measurements.

1.1 Research Gap

Hydrodynamic data is used to make predictions about, for example, the effects of sea level rise and migrating bedforms. However, this data is often of insufficient quality for its intended purpose or has a low spatial resolution. This means that new methods of obtaining hydrodynamic data should be considered. One of the possible solutions is making use of ship-based DVL measurements. These measurements have a high quality and a large temporal and spatial resolution. However, these measurements vary both in space and time and no methods are currently available to go from these measurements to a hydrodynamic model of high quality and high temporal and spatial resolution. The lack of these methods forms the basis of this research.

1.2 Research Objective

The aim of this master thesis is to:
Construct a mathematical/semi-empirical model that gives an expression of the flow velocity and direction at multiple locations and water depths in a marine environment for a specific time, based on ship-based DVL measurements.

This model will be semi-empirical, meaning that the model uses DVL measurements, but the predictions made also depend on physical processes. This means that the model is not entirely data-driven, but also not fully based on physical processes. Hence, a model needs to be developed based on both the available data and using expressions representing physical processes. This leads to the main research question:

In what way can a semi-empirical model be developed to express flow velocities and directions in a marine environment, based on ship-based DVL measurements?

To do this, first, the available DVL measurements need to be analysed and filtered to be able to be used as input for the hydrodynamic model. Next, the model will be developed by taking the most important factor affecting the flow velocities, the tides, into account. The developed model will finally be validated by looking at other existing hydrodynamic data sources such as buoy measurements and the output of the DCSM to see how the model output compares to the other data sources. This yields the following sub-questions:

- *How can the DVL data be used as input for a hydrodynamic semi-empirical model?*
- *What semi-empirical model can be developed for flow velocities and directions in a marine environment?*
- *What differences exist with other flow velocity data sources?*

Finally, the answers to these research questions will lead to an answer to the main research question. This will provide a final model that can use ship-based DVL measurements in a marine environment to predict tidal flow velocity and direction. The model will then be evaluated for possible shortcomings and improvements and recommendations will be made to improve the way the ship-based DVL measurements are now collected.

The scope of this project is as follows:

- Analysing and filtering the available DVL data.
- Developing a hydrodynamic model based on DVL measurements in the North Sea.
- Including the tidal components in the semi-empirical model.
- Validating the model based on other data sources in the North Sea.

This means that, while the goal is to develop a model that generally works in a marine environment, the model is only developed and tested based on measurements made in the North Sea. Testing the model on other marine environments is not included in this project's scope.

1.3 Structure of the report

The outline of the steps taken in this report can be seen in Figure 1. As can be seen in this figure, first a theoretical background will be provided based on available literature. Next, a description of the data set provided by the Royal Netherlands Navy will be given and the steps taken in the pre-processing of the data are shown. After this, the general methodology to develop the model will be discussed, where the techniques, such as T-Tide, used for the harmonic analysis will be introduced. The next step is the model development, where the implemented approach for the tidal propagation based on the tidal signal will be explained, for which two methods are introduced. The output of these two methods will be analysed using the provided data. Thereafter, the output will be validated based on a verification of the harmonic analysis and a comparison with the DCSM and buoy measurements. This will be followed by a discussion comparing the developed methods with other research. Also, shortcomings and further research for this project will be mentioned and the research questions will be answered in the conclusion. Finally, some recommendations will be made for the Royal Netherlands Navy and other people interested in this project in what way the provided ship-based DVL measurements can be improved and how to continue with this project.

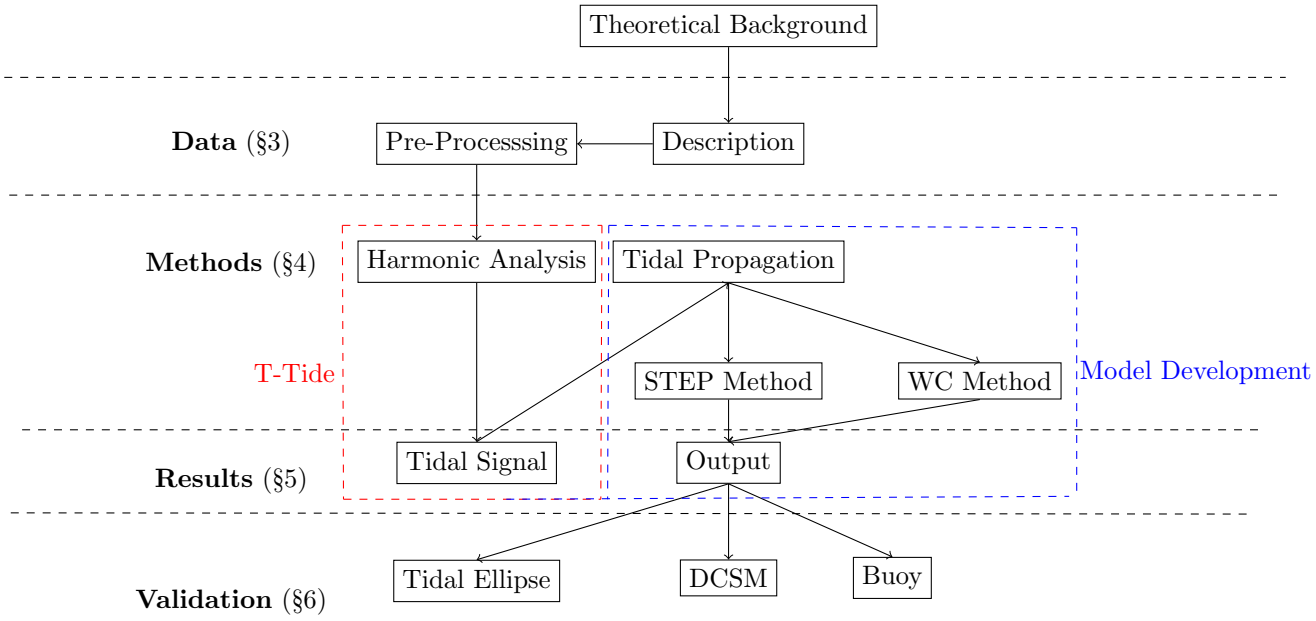

Figure 1: Outline of the structure of the report.

2 Theoretical Background

First, a background, based on literature, will be given about the working of a DVL, after which the analysis of the tidal signal will be discussed.

2.1 Doppler Velocity Log (DVL)

The DVL used by the Royal Netherlands Navy, specifically a DVL500 from Nortek, is primarily used for subsea navigation. Other ways of navigation, for example by using satellites, do not work underwater. The

DVL can be used as an extension for other navigation sources to overcome this problem. To do this, the DVL measures the velocity of the ship relative to the sea bed by emitting sound pulses. This velocity can then be used together with the time step between two measurements to get the displacement relative to the seabed, which can then be used for navigation (Nortek, 2023a).

As mentioned before, a DVL can also be used in the same way as an ADCP. An ADCP is a commonly used device to measure hydrodynamics and can be used to measure the velocity profile over the complete water column, combining both waves and currents (Pandian et al., 2010), and to measure the near-bed velocity profile, which can be used to analyse the tidal flow and the wave orbital motion (Elias, 2017; Van Prooijen et al., 2020). ADCPs with high sampling frequency can also be used to estimate turbulence parameters such as the Reynolds stresses and turbulent kinetic energy dissipation rates (Guerra and Thomson, 2017). An example of where ADCP measurements are used to determine the structure of turbulent flow is a case study for the Ohta estuary in Japan (Kawanisi, 2004). One of the main advantages is that an ADCP yields an accurate velocity profile instead of a point measurement given by other commonly used methods, such as an ADV (Acoustic Doppler Velocimeter)(Horstman et al., 2011). A disadvantage is that in the intertidal area, ADCPs may yield unexplainable peaks in the data caused by interference with present vegetation (Horstman et al., 2011). Furthermore, in the case of a combination of large water depth and small wave heights, the wave height predictions of an ADCP are unreliable (Schrijvershof et al., 2019). In areas with low water, the ADCP can get exposed, causing there to be no data (Elias, 2017), and varying water levels lead to noise since one reference water level has to be set before deploying an ADCP (Horstman et al., 2011). Another disadvantage is that ADCP measurements are not always optimally located (Pandian et al., 2010) and lack spatial information (Van Gils, 2014). Using a ship-based ADCP can overcome this lack of spatial information. Looking at the accuracy, it can be seen that ship-mounted ADCP measurements have errors of 6% for the velocity magnitude and up to 3° for the direction (Fong and Monismith, 2004).

The minimum accuracy of the DVL, when used as an ADCP, for measuring flow velocities is 0.3% $\pm$ 0.3 cm/s (Nortek, 2023a), which is the same as for an ADCP developed by Nortek (Nortek, 2023b). However, since the primary use is navigation the DVL is not ideally configured to make flow velocity measurements, meaning that the accuracy of these measurements is lower. While measuring, the DVL identifies whether a measurement becomes invalid or not. This is done by looking at the signal-to-noise ratio, which indicates the strength of the tidal signal measured by the DVL compared to the background noise of the measurements, and by looking at the correlation between a new measurement and the previous one. Flow velocity measurements made by the DVL become invalid if the signal-to-noise ratio is lower than the noise level or if the correlation between measurements is lower than 50% (Nortek, 2023c).

2.2 Tidal Signal Analysis

The tides are one of the main forcing terms for the flow velocity in a marine environment, and the tidal variability is often the largest signal in an oceanic time series (Pawlowicz et al., 2002). The astronomical forcing of the tides can be written as a linear combination of sinusoidal terms each having a distinct amplitude, phase, and frequency (Doodson, 1921). The oceanic response to the astronomical forcing is similar, each sinusoid is a tidal constituent, with the same frequency as for the astronomical forcing but with varying amplitudes and phases, which is known as classical harmonic analysis (Foreman and Henry, 1989). Hence, a tidal time series can be expressed as

$$y_i = A_0 + \sum_{j=1}^{M} A_j \cos\left(\sigma_j t_i - \Phi_j\right), \tag{1}$$

where y_i is the observation at time t_i, A_0 is a small background velocity, M is the number of tidal constituents chosen in the analysis and A_j, σ_j, Φ_j are the amplitude, frequency and phase of constituent j respectively (Foreman and Henry, 1989). It is, however, unfeasible to select all tidal constituents, since this can lead to an ill-conditioned equation causing the solutions to have a large confidence interval. One approach that can be taken to get the amplitude, frequency, and phase from this system of equations is a least-squares approach (Foreman and Henry, 1989). Here, the optimal solution for each parameter value is found by minimizing the squared sum of the difference between the fitted and observed value. One important hydrodynamic time scale is the spring-neap cycle, caused by the semi-diurnal lunar and solar tidal components, where there are lower flow velocities during neap tides and higher flow velocities during spring tide. The spring-neap cycle has a period of 14.8 days. To include this in the model, the semi-diurnal lunar and solar tidal components need to be included in the harmonic analysis (Stephenson, 2016).

Classical harmonic analysis has several drawbacks. First of all, to resolve all frequencies for the tidal constituents a time series of 18.6 years is needed, since then all tidal constituents have completed at least one cycle and have synced up again. Therefore, often the assumption is made that sinusoids with similar frequencies share proportional phase and amplitude characteristics with the equilibrium response, which is the phase and amplitude that would be observed if the ocean was in equilibrium with the tidal forcing. If the equilibrium response is known the behaviour of the tidal constituents with these frequencies can then be predicted (Pawlowicz et al., 2002). This will lead to a total signal looking like a sinusoid with a slowly varying phase and amplitude. For time series of up to one year, both can be assumed to be constant. For shorter time series another problem may arise causing the constituents to be unresolvable because no distinction can be made between constituents with similar frequencies. This can be solved by applying interference, which requires that the relative difference between the unresolved tidal constituents is known from other nearby data sources. If this is not known the smaller constituents should be discarded or the equilibrium response should be used to determine the relative difference (Pawlowicz et al., 2002). Another problem with classical harmonic analysis may arise in coastal regions where the tides resemble a wave propagating onshore. Seasonal variability in salinity and flow in estuaries can cause the tidal processes to not be constant over time. As long as this variability can be estimated deterministically, this can be solved by adding extra shallow-water tidal constituents, which can be used as a representation of this variability (Pawlowicz et al., 2002).

3 Data

3.1 Description

For this project, two different data sets were provided by the Royal Netherlands Navy. These data sets were measured by using a DVL mounted on the ship Zr.Ms. Snellius. The data sets consist of the flow velocity vector, $\mathbf{v}$, in m/s and the flow direction α in degrees at different water depths in the North Sea ranging from 0 to 42 m, with increments of 2 m, plus the draught of the ship, which is 4 m. This means that the flow velocities provided are measured at the middle of each increment, meaning at a depth of 5 m, 7 m and so on. A new measurement is made every 10 seconds. These measurements are made while the ship is sailing, meaning that besides a temporal difference in the measurements, a spatial difference in the measurements is present.

The flow velocity vector can be represented as a complex velocity time series:

$$\mathbf{v} = |\mathbf{v}|(\cos\alpha + i\sin\alpha) = u + iv, \tag{2}$$

where u is the eastward velocity and v is the northward velocity and i is the imaginary number. This means that:

$$\begin{aligned} u &= \mathbf{v}\sin\alpha, \\ v &= \mathbf{v}\cos\alpha. \end{aligned} \tag{3}$$

The first data set provided consists of measurements made between August 24 and September, September 12 and 16, September 19 and 22, and October 25 and 31, 2022. However, the data is all invalid between August 29 and September 6, since the ship was docked in the harbour, but the DVL was still activated. The location of the performed DVL measurements for this data set is visible in Figure 2. The measured velocities and directions are rounded to one decimal in this data set. The second data set contains similar data as the first and includes data recorded between 16 and 21 May 2023. The locations of the measurements can be seen in Figure 3. The measured flow velocities and directions are now rounded to four decimals. Besides this, the new data set provides the ground track of the DVL, which is the path on the seabed, the wind speed, and the wind direction at each location.

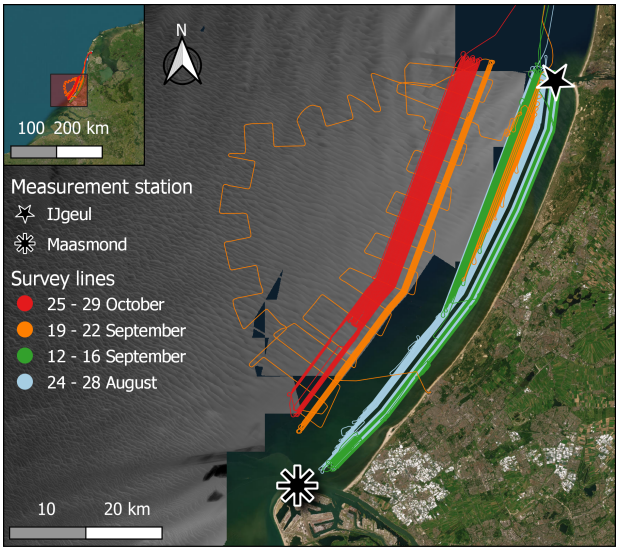

Figure 2: First set of DVL measurements made by the Royal Netherlands Navy in 2022.

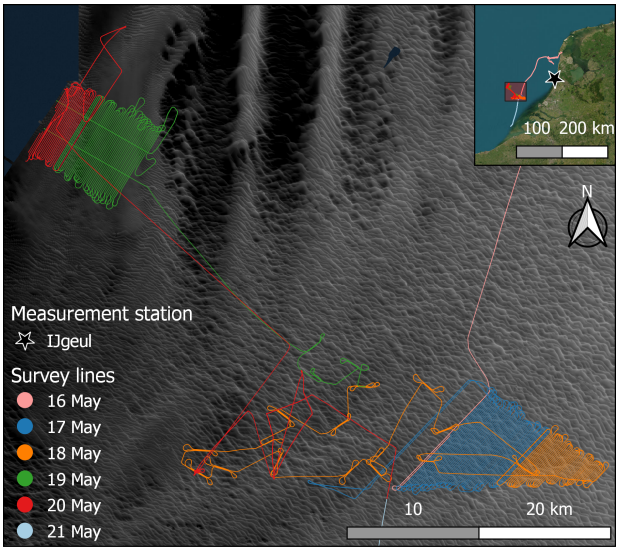

Figure 3: Second set of DVL measurements made by the Royal Netherlands Navy in 2023.

For both data sets the eastward and northward velocities are calculated using Equation 3. Plotting the tidal ellipse for each data set yields Figure 4. Here, it can be seen that the main direction of the measured velocities for both data sets is similar, but that the magnitude of the velocities is larger in 2022. Furthermore, it can be seen that all measurement points from 2022 lie on circles, with radii of multiples of 0.1 m/s. This is caused by the rounding of the measured flow velocities and directions. This has the effect that all small-scale effects on the velocities are filtered out and therefore can not be analysed. Also, since the order of magnitude of the measurements is around 1 m/s and the DVL has an accuracy of 0.3% $\pm$ 0.3 cm/s, the DVL is able to measure the flow velocities accurately up to 3 decimals. Hence, the DVL is able to measure more accurately than is done in this data set. Because of the lack of significant digits, this data set unfortunately is not useful to create an accurate model. Looking at the data set for 2023 no large gap is present between the data points in the tidal ellipse. This makes it more likely that small-scale processes are included in this model. Hence, this data set is more suitable to use for developing a model, and therefore, in the rest of this study, only the second data set is taken into account.

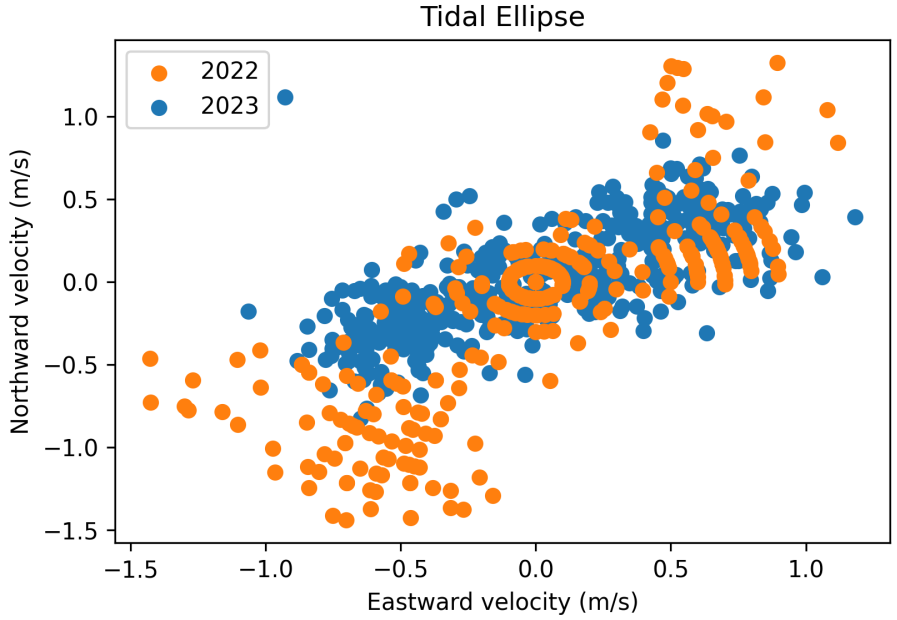

Figure 4: Tidal ellipses based on a sample of both data sets.

3.2 Pre-Processing

Of course, the data set still includes some errors and outliers that need to be filtered out, before a harmonic analysis can be applied. First of all, the known errors in the measurements will be discussed, after which the filtering of the outliers is explained.

3.2.1 Errors in the Measurements

First of all, the DVL indicates whether a measurement is valid or invalid, by looking at the signal-to-noise ratio and correlation of the measurements. Hence, only all valid measurements need to be considered. Secondly, the top layer of measurements is affected by turbulence caused by the ship. To deal with this the top 2 m of the measurements, need to be filtered out of the data set (Huitema, personal communication, June 1, 2023).

Next, the bottom part of the measurements is affected by the sidelobes of the DVL. This means that all measurements in the bottom 10% of the water column above the seabed need to be filtered out. Since the provided data set also yields (invalid) flow velocity values below the sea bed, it is not directly clear from the data set where the bottom of the sea bed is. To deal with this, a bathymetry data set with a resolution of 25 m, provided by the The Netherlands Hydrographic Service (2023), of the study area is used to check the approximate depth near each measurement location, based on the closest bathymetry data point to the measurement location. Next, the bottom 10% of the water column is excluded. If the bottom 10% of the water column is included, part of the signal, the side lobes, will interfere with the seabed, meaning that these measurements will be inaccurate (Huitema, personal communication, June 1, 2023).

3.2.2 Time Log Difference

Another issue is that the internal clocks of the DVL and the software on the ship, Qinsy, were not synchronized. Qinsy is responsible for the postprocessing of the data, which means that corrections are applied to the measurements for the heading, pitch, and roll of the ship. Since the internal clocks were not synchronized there is a difference in the time on the DVL and in Qinsy, meaning that corrections are applied at the wrong moment. Also, this possible difference might not be constant, since there is a small drift in the internal clock, causing a small offset in the timing of the measurements and hence the possible difference to change over time (Huitema, personal communication, June 1, 2023). This means that the corrections applied are likely incorrect. For the pitch and roll, this is a large issue since the pitch and roll can differ quite a lot in a few seconds time due to wave effects. Unfortunately, this can not be solved, since the possible offset between the internal clocks is not known, hence in the rest of this report the assumption is made that the pitch and roll corrections applied are not very influential. In the case of small waves, the error caused by the pitch and roll corrections will be smaller compared to the case of large waves. During the period the DVL measurements were made, the wave climate was relatively calm (Rijkswaterstaat, 2023), making the assumption more reasonable. This assumption will not influence the methods applied in the development of the model but will have an effect on the analysis of the results, because of the mistake in pitch and roll corrections. The possible offset for the heading correction can be dealt with by only considering the moments the ship is sailing in a straight line since the heading of the ship at those moments is approximately constant. This means that the moments when the ship is changing direction should be left out. Still, this remains an assumption, since the offset in the internal clocks might be so large that a heading correction is made for the scenario that the boat is changing direction, but actually, the ship is sailing in a straight line. The way this data is filtered out is by looking at the direction the ship is sailing between two measurement points with respect to the true north and comparing this with the direction the ship had before. If a sudden change in direction is visible, these data points are left out of the model.

3.2.3 Outliers

Besides filtering out all errors related to the device set-up in the data set, it is also important to filter out other, measurement-related, outliers in the data. This is done by calculating the mean tidal signal for batches of 10 minutes. This takes multiple data points into account for filtering, and at the same time does not take too large batches preventing the deviations within the batch from getting too large. Overlapping batches are applied because, without overlapping batches, each batch covers a specific time range, for example, one batch from 00:10:00 to 00:20:00 and another from 00:20:00 to 00:30:00. If there are measurements at 00:19:50 and 00:20:10, they would end up in different batches. By introducing overlapping batches, you create a zone where these measurements overlap, such as from 00:15:00 to 00:25:00. This ensures that measurements

occurring close in time, like 00:19:50 and 00:20:10, are included together in a batch. This way, the model can consider the correlation between these measurements, which is important for accurate analysis. For each batch, the standard deviation is calculated. A data point is filtered out when a measurement inside this batch differs from the mean by a certain amount of standard deviations. Here, it has to be noted that the lower bound for the velocity magnitudes is 0 since magnitudes always have to be positive. The number of standard deviations considered will be determined by testing multiple cases to see which amount of deviations keep almost all relevant data points while filtering out the obvious outliers.

Furthermore, the filtering of outliers is performed three times. First of all, for the velocity magnitude data coming directly from the DVL. Next, the filtered velocity magnitudes and the unfiltered velocity directions are used to calculate the northward and eastward velocity magnitudes by using Equation 3, which are then filtered using the same process. Several values for the standard deviation have been tested to see for which standard deviation most of the signal is preserved while the obvious outliers get removed. These tests showed that four standard deviations give the desired result in the filtering process. Below the filtering process is visualised using four standard deviations as the upper and lower boundary. In Appendix A.1, the filtering process is shown for different values for the standard deviation.

This filtering process is visualised in Figure 5. In this figure, there is zoomed in on 20 minutes of the filtering process. Here, it can be seen that there are four batches within this time interval. In this time range, there is one outlier for the velocity magnitude since one data point of the original time series is out of bounds. Hence, this data point has been filtered out by setting it as a NaN-value.

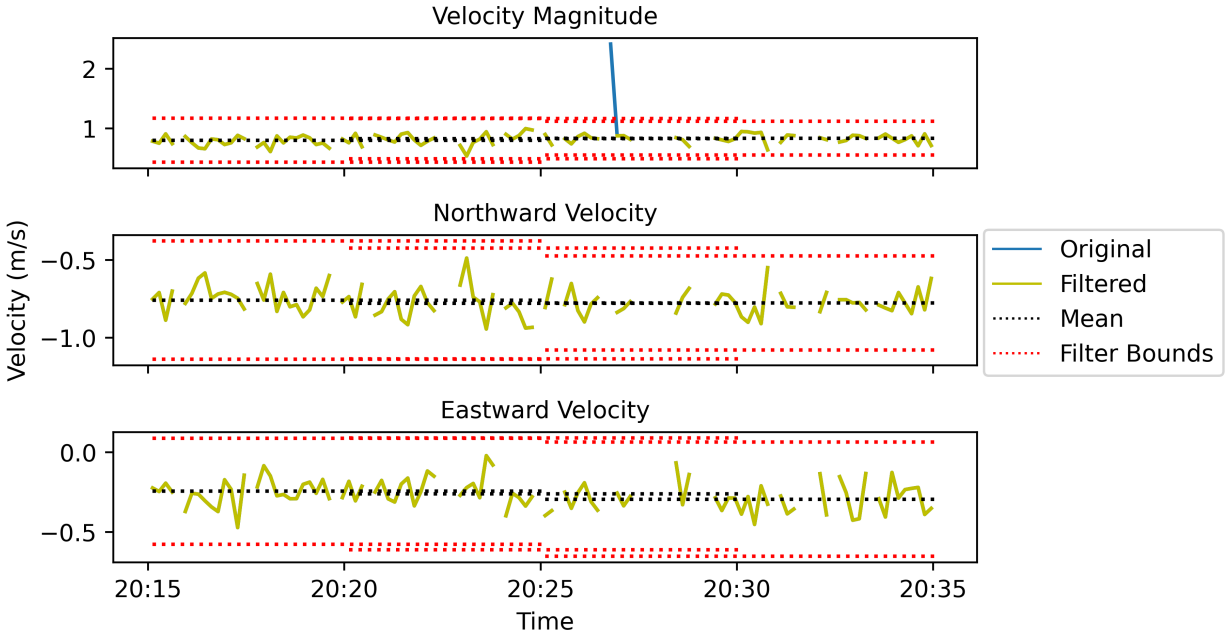

Figure 5: Filtering process zoomed in on 20 minutes based on bounds set at 4 standard deviations with respect to the mean velocity at a water depth of 7 m. Shows an outlier in the original time series in the velocity magnitude times series around 20:27. Mean and filter bounds are plotted from 20:15 until 20:25, from 20:20 until 20:30 and from 20:25 until 20:30.

Looking at the complete time series, which can be seen in Figure 6, it can be seen that especially in the velocity magnitude time series more outliers are filtered compared to the north- and eastward velocity time series because these time series already make use of the filtered velocity magnitudes.

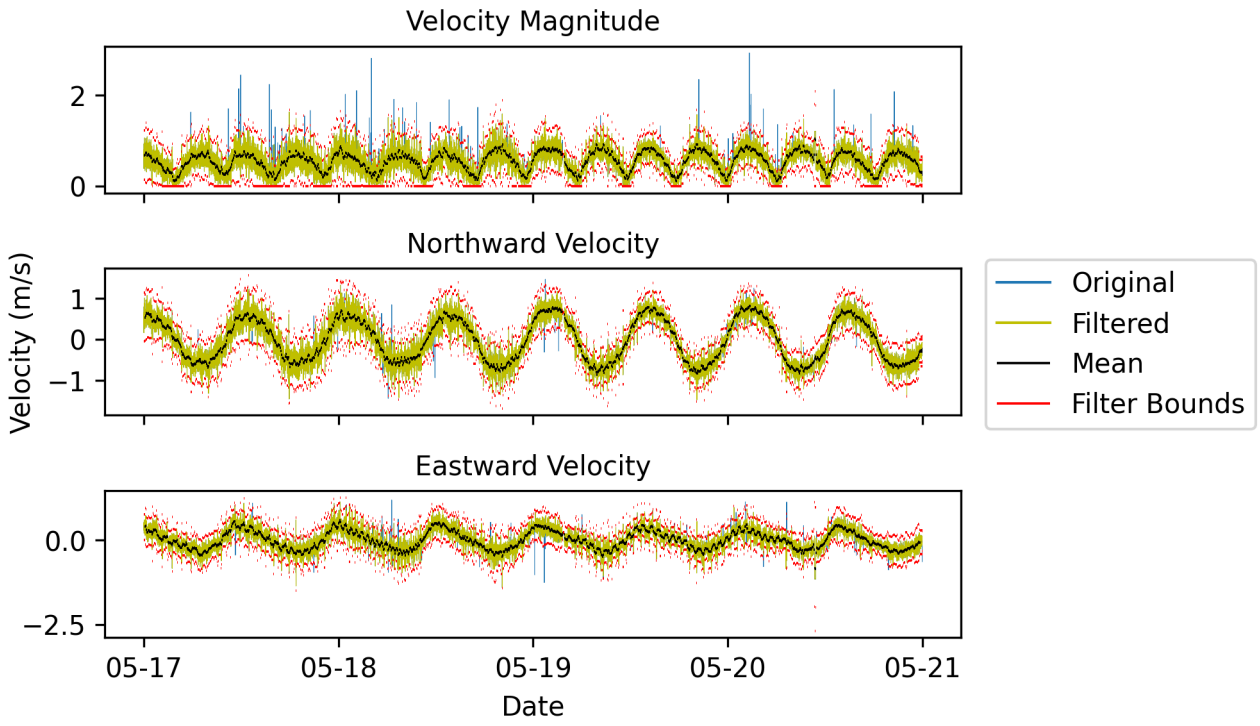

Figure 6: Filtering process for a complete time series based on bounds set at 4 standard deviations with respect to the mean velocity for overlapping batches of 10 minutes at a water depth of 7 m.

To get an indication of the amount of data points that have been filtered out by this process, the total number of outliers and the percentage of outliers for the velocity magnitudes and the northward and eastward velocities are calculated for all depth layers combined. This is shown in Table 1. To get the percentage of the total number of data points, only the data points are considered that are not changed into NaN values in the previous pre-processing steps. As can be seen in this table, the amount of outliers for the north- and eastward velocities is the same, because this shows the filtering on the velocity direction and if one of the two is an outlier the other velocity is also incorrect, since this indicates that the direction value was an outlier. Furthermore, the amount of outliers for the velocity magnitude is higher compared the northward and eastward velocities, which could also be seen in Figure 6.

Table 1: Total number and percentage of outliers

	Number of outliers	Percentage of outliers
Velocity Magnitudes	2208	0.16%
Northward Velocities	1355	0.098%
Eastward Velocities	1355	0.098%

3.3 Multilayer Depth Model

The filtered data now still contains the flow velocities for each depth layer of measurements. For the outputs discussed in the rest of this report, the choice has been made to not look separately at the output of each depth layer but to combine the depth layers into one. However, to do this, the effect of the sea bed on the flow velocity measurements should not be taken into account. The interaction with the seabed creates a boundary layer above the seabed, whose width depends on factors like the bed roughness and the flow velocity magnitude and can lead to turbulence, which affects the flow velocities above the seabed (Singh et al., 2016). Since this mainly influences the bottom part of the water column and not the entire water column, this layer will be filtered out to get a depth-averaged flow velocity. To determine where the split point between this layer needs to be, the velocity profiles based on the velocity magnitude are plotted for different time periods of the filtered data. Based on these velocity profiles, it can be checked at what water depth there is a sudden change in the shape of the velocity profile. The water depth where this occurs most often is then chosen as the split level for the top and bottom layers. Since for each measurement location,

the water depth is different, the velocity profile and hence the split point for the velocity profile changes at each location. Hence, to determine the split level, the maximum split level will be chosen, so that the depth of the top part of the water column is constant. The bottom layer will have a varying depth because of the changing bathymetry. Based on this split an average flow velocity will be computed for the top and bottom layers, which will then be used further in the model.

To determine where the split should be between the top and bottom part of the water column, the velocity profiles are plotted for three different moments in the tidal wave. First, the velocity profile is considered at the time the velocity magnitude is at its largest in the tidal wave, shown in Figure 7. Here, the velocity magnitude is averaged based on 200 measurements, to filter out points where the behaviour of the velocity profile is not as expected. In this figure, a transition in the velocity profile is visible at -26.8 m. Here, in the bottom part of the water column, the velocity magnitude increases. This can be caused by turbulence affecting the measurements near the sea bed. In the top part of the water column, the velocity magnitude increases when coming closer to the water level. This is caused by the Coriolis effect, causing there to be a phase difference between the top and the bottom of the water column (Fang and Ichiye, 1983). This means that the tidal wave in the bottom part is a bit behind the tidal wave in the top part of the water column, meaning that in the bottom part of the water column the peak velocity magnitudes have not yet been reached.

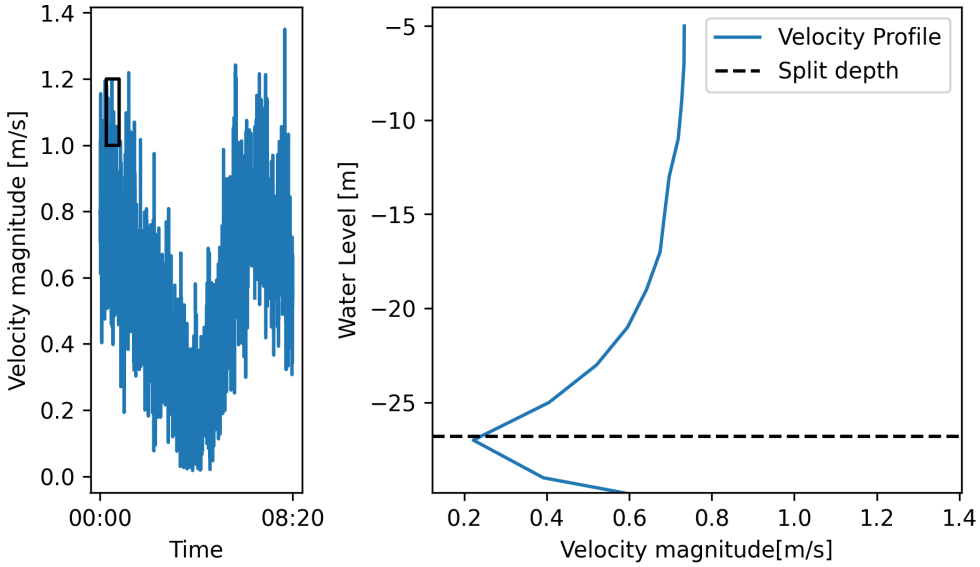

Figure 7: In the left panel the filtered velocity magnitude is plotted between 00:00 and 08:20 on May 17 at a water level of -5 m. The black box indicates the measurements on which the velocity profile in the right panel is based. The right panel shows the velocity profile for the highest velocity magnitude values. The split depth indicates the water level where the transition in the velocity profile takes place.

Looking at a moment between high and low velocity magnitudes, shown in Figure 8, shows a split in the velocity profile at -25 m. Below this split level, the measured velocities magnitudes are smaller, which is caused by the effects of the bottom friction in the bottom layer of the water column. Above the split level, a slight decrease in the velocity magnitudes is visible. This is again caused by the Coriolis effect and the difference in the tidal phase of the bottom part of the water column. In the bottom part of the water column, the tidal wave is lagging behind, causing there to be higher flow velocities in this part of the water column.

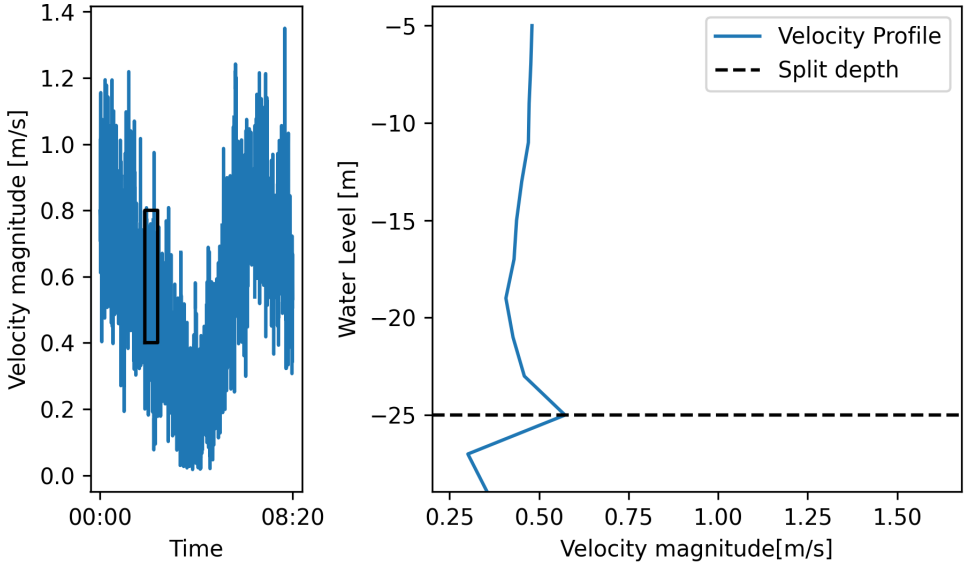

Figure 8: In the left panel the filtered velocity magnitude is plotted between 00:00 and 08:20 on May 17 at a water level of -5 m. The black box indicates the measurements on which the velocity profile in the right panel is based. The right panel shows the velocity profile for average velocity magnitude values. The split depth indicates the water level where the transition in the velocity profile takes place.

Finally, looking at the moment with low velocity magnitudes, hence the moment the tide is turning, shown in Figure 9, a split is shown at -25 m. Again, below this level, the velocity magnitudes are smaller, caused by the bottom friction of the seabed in the boundary layer. Also, a decrease in velocity magnitudes is visible when coming closer to the water surface, caused by the Coriolis effect. Again, in the bottom part of the water column, the tidal wave is lagging behind, meaning that in the bottom part of the water column, the minimum velocity magnitudes have not yet been reached.

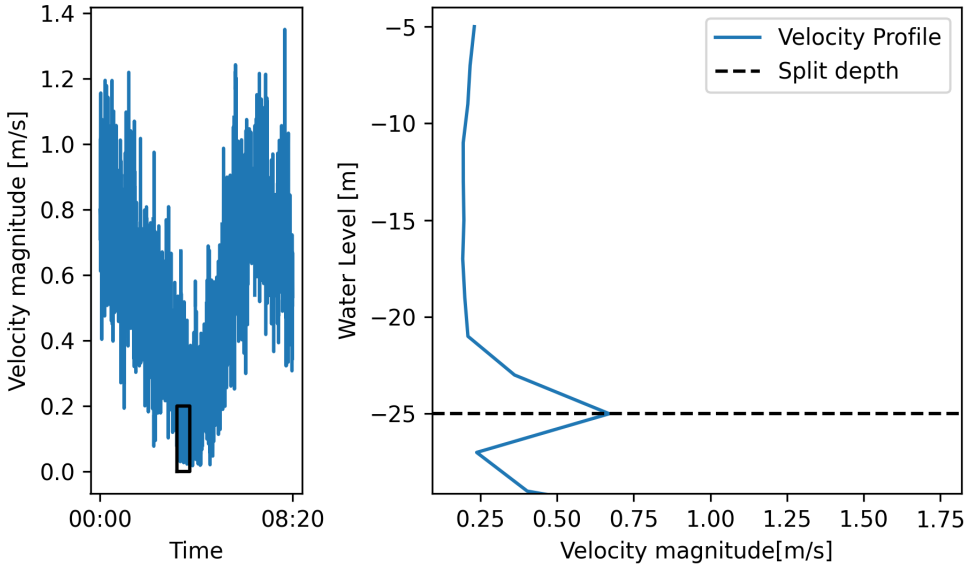

Figure 9: In the left panel the filtered velocity magnitude is plotted between 00:00 and 08:20 on May 17 at a water level of -5 m. The black box indicates the measurements on which the velocity profile in the right panel is based. The right panel shows the velocity profile for minimum velocity magnitude values. The split depth indicates the water level where the transition in the velocity profile takes place.

Based on these velocity profiles, the choice has been made to make a split in the water column at a water level of -25 m, to exclude the effects of the seabed on the velocities. Here, it has to be noted that this split can be adjusted based on what is needed. This means that if only measurements are needed for a certain range in the water column, this can easily be adjusted. Furthermore, it is not needed to make this split. The model introduced below also works when applied to a certain depth layer. However, to generalize the results, a depth-averaged approach has been taken, when testing the model output.

4 Methods

In this section, the methods used to develop the model are discussed. First, the techniques used for the harmonic analysis will be discussed after which the grid will be explained and finally, two methods to implement the tidal propagation are introduced.

4.1 Harmonic Analysis

One of the tools available to perform the classical harmonic analysis is the MATLAB toolbox `T_Tide` developed by Pawlowicz et al. (2002), which separates the non-tidal signals from the tidal signals in an oceanic time series, and is also able to address the problems that arise when using classical harmonic analysis by applying interference or adding shallow water constituents (Pawlowicz et al., 2002). The separation of the tidal signals from the non-tidal signals is done by calculating the frequency of the included tidal constituents and based on this estimate the tidal amplitude of this tidal constituent in the time series. Using harmonic analysis, `T_Tide` makes estimates of the amplitude and phase of each of the included tidal components and the error in these estimates. If the signal-to-noise ratio for a tidal constituent is large enough, meaning the errors are small enough, this tidal constituent is deemed significant. Simulations on a fixed data set showed that a signal-to-noise ratio of 2.0 or higher is deemed good enough for a tidal constituent to be significant (Pawlowicz et al., 2002). By combining all significant tidal constituents, `T_Tide` divides the original time series into a tidal time series and a residual time series, which is the leftover signal after the tidal time series is subtracted from the original time series (Pawlowicz et al., 2002). This software is able to automatically select relevant tidal constituents for the analysis.

`T_Tide` requires as input a complex velocity time series, the time step, the latitude of the measurement area, and the minimum signal-to-noise ratio. Using the filtered data as input data in `T_Tide`, when performing the harmonic analysis, the assumption is made that all measurements are made at the same point, instead of with a sailing vessel. In case more data is available, the data set can be separated into multiple data sets, so that the tidal ellipse parameters are provided at multiple locations. However, with the data set provided by the Royal Netherlands Navy, the time series is too short to be separated into multiple time series while still maintaining the most important tidal constituents as output from the harmonic analysis. This will result in the output of the harmonic analysis being constant over the entire model domain. No similar studies have ben found using the same assumption when using `T_Tide`, hence the results of the harmonic analysis for each grid cell should be verified to make sure that this assumption is valid. The output for tidal constituent j considered in the harmonic analysis is the major axis of the tidal ellipse R_j, which represents the direction of the strongest tidal current flow, and the minor axis r_j, which represents the direction of the weakest tidal current flow. Furthermore, the harmonic analysis yields the inclination of the tidal ellipse with respect to the true north, θ_j, the phase ϕ_j at time 0, which indicates how far along the tidal cycle the tidal wave is at the start of the time series, the angular frequency σ_j, which is the number of cycles in a given time, and the signal-to-noise ratio snr_j. A schematisation of a tidal ellipse is shown in Figure 10.

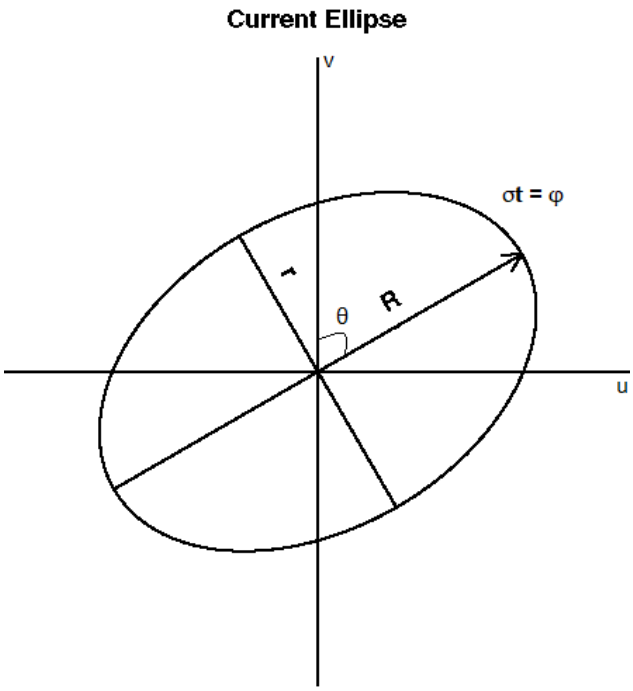

Figure 10: Schematisation of a tidal ellipse. Here, v is the northward velocity, u is the eastward velocity, r is the minor axis of the tidal ellipse, R the major axis, θ the angle of inclination with respect to the true North, σ the angular frequency, t the time and ϕ is the phase.

Since the harmonic analysis assumes that the measurements are made at one location, the tidal ellipse parameters are the same over the complete study area and hence not dependent on the x and y location.

4.2 Grid

To be able to make a model of the tidal velocities in the model domain, a grid needs to be defined over the model domain. The size of the grid cells can be adjusted based on what is desired. By doing this, a grid cell can contain multiple measurements, but some cells might not contain a measurement at all. Since inside each grid cell with measurements, multiple measurement locations are present, it needs to be identified which measurements are made in which grid cell by looking at the coordinates of each measurement. For each grid cell, the measurements are then saved. Furthermore, since the ship can sail through the same grid cell multiple times, the saved measurement points for each grid cell need to be split into groups of successive measurements. Using the successive measurements, an average flow velocity and direction for that grid cell can then be calculated at the average timestamp of those measurements.

Since the model is based on the data set shown in Figure 3, a grid needs to be defined for this model area, so that each set of subsequent velocity measurements in a grid cell will be translated to an average velocity vector for that set of measurements at the average time of these measurements. An example grid can be seen in Figure 11. This grid is the same grid used for the comparison with the DCSM and will be used to explain the output of the model. However, the size of each grid cell can easily be adjusted to match the desired output, An example can be seen in Figure 12, where the grid size is smaller for a case where a higher spatial resolution is needed for the flow velocity predictions.

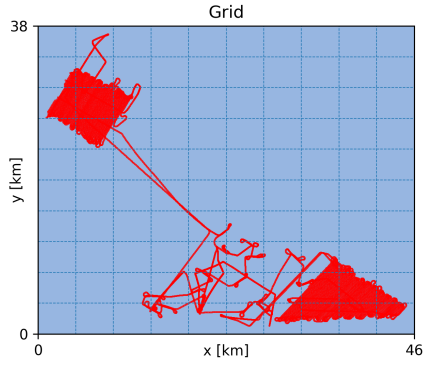

Figure 11: Example grid of grid cell with a width of 4618 m and a height of 3787 m.

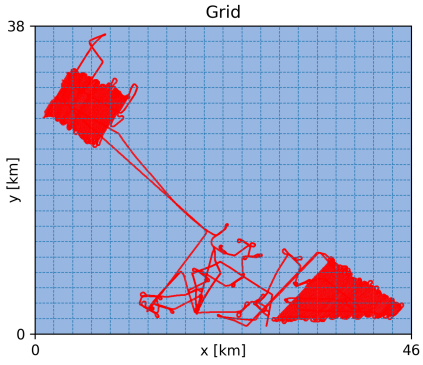

Figure 12: Example grid with grid cells with a width of 2309 m and a height of 1893 m.

4.3 Tidal Propagation

The significant tidal constituents are determined using harmonic analysis. Using these tidal constituents, the tidal propagation between two grid cells can be calculated. Slightly rewriting the tidal wave propagation in Equation 1 in the eastward and northward velocity components, as shown in Section 2.2, for tidal constituent j yields:

$$\begin{aligned} u_j(x,y,t) &= u_{j,0}(x,y,t) + A_{j,u}(x,y)\cos\left(\phi_{j,u}(t) + 2\pi\sigma_j\Delta t - \Delta\phi_{j,u}(x,y)\right), \\ v_j(x,y,t) &= v_{j,0}(x,y,t) + A_{j,v}(x,y)\cos\left(\phi_{j,v}(t) + 2\pi\sigma_j\Delta t - \Delta\phi_{j,v}(x,y)\right). \end{aligned} \tag{4}$$

Here, u_j is the eastward velocity in m/s of tidal constituent j, v_j is the northward velocity in m/s of tidal constituent j, $u_{j,0}$ is an eastward reference velocity in m/s, $v_{j,0}$ is a northward reference velocity in m/s, $A_{j,u}$ is the amplitude of the eastward velocity of tidal constituent j in m/s, $A_{j,v}$ is the amplitude of the northward velocity of tidal constituent j in m/s, $\phi_{j,u}(t)$ is the phase of the northward velocity at time t in degrees and $\phi_{j,v}(t)$ is the phase of the northward velocity at time t in degrees. In Equation 4, the term $\phi_{j,u}(t)$ represents the moment in the tidal wave the eastward tidal wave is in at time t, $2\pi\sigma_j\Delta t$ represents the number of degrees the tidal wave has gone through during a time span of Δt and $\Delta\phi_{j,u}(x,y)$ is the difference in phase of the tidal wave with respect to another location. The amplitude and phase at time 0 for the northward and eastward velocity can be calculated using the tidal ellipse variables obtained in the harmonic analysis (Xu, 2000):

$$\begin{aligned} A_{j,u} &= \left|w_{j,p} + w_{j,m}\right|, \qquad \phi_{j,u}(0) = -\arg(w_{j,p} + w_{j,m}), \\ A_{j,v} &= \left|w_{j,p} - w_{j,m}^*\right|, \qquad \phi_{j,v}(0) = -\arg\left(\frac{w_{j,p} - w_{j,m}^*}{i}\right). \end{aligned} \tag{5}$$

where $w_{j,m}^*$ denotes the complex conjugate of $w_{j,m}$. The newly introduced parameters $w_{j,m}$ and $w_{j,p}$ can then be calculated from the tidal ellipse parameters, using:

$$\begin{aligned} w_{j,p} &= W_{j,p}e^{-i\theta_{j,p}}, \qquad w_{j,m} = W_{j,m}e^{i\theta_{j,m}}, \qquad W_{j,p} = \frac{1+\frac{r_j}{R_j}}{2}R_j, \\ W_{j,m} &= \frac{1-\frac{r_j}{R_j}}{2}R_j, \qquad \theta_{j,p} = \frac{\pi}{2} - \theta_j - \phi_j, \qquad \theta_{j,m} = \frac{\pi}{2} - \theta_j + \phi_j. \end{aligned} \tag{6}$$

Using Equation 5, the phase at time t can be calculated using:

$$\begin{aligned} \phi_{j,u}(t) &= \phi_{j,u}(0) + 2\pi\sigma_j t, \\ \phi_{j,v}(t) &= \phi_{j,u}(0) + 2\pi\sigma_j t. \end{aligned} \tag{7}$$

Using the calculated amplitudes from Equation 5 and the calculated phases from Equations 7, yields an estimation of the tidal currents of each constituent at time t, assuming reference velocities $u_{j,0} = 0$ m/s and

$v_{j,0}$ m/s.:

$$u_j(x,y,t) = A_{j,u}\cos(\phi_{j,u}(t) + 2\pi\sigma_j\Delta t - \Delta\phi_{j,u}),$$
$$v_j(x,y,t) = A_{j,v}\cos(\phi_{j,v}(t) + 2\pi\sigma_j\Delta t - \Delta\phi_{j,v}). \tag{8}$$

To calculate the tidal velocities in another grid cell, two methods are implemented in the model, the Spatial-from-Temporal Estimated Phase (STEP) Method and the Wave Celerity (WC) Method:

4.3.1 Spatial-from-Temporal Estimated Phase (STEP) Method

The first method uses the fact that the temporal difference between two measurements can be calculated. Imagine that in grid cells A, B, and D, there are measurements at times t_0, t_1, and t_3 and average measurement location m_A, m_B and m_D, respectively, as shown in Figure 13. The average measurement locations are determined by calculating the average location of all subsequent measurements in one grid cell. Furthermore, grid cell C has no measurements. At time t_0, there is only a flow velocity in grid cell A, but the goal is to have an estimation for the flow velocity in the middle of all grid cells at this time. To get this, three steps are taken:

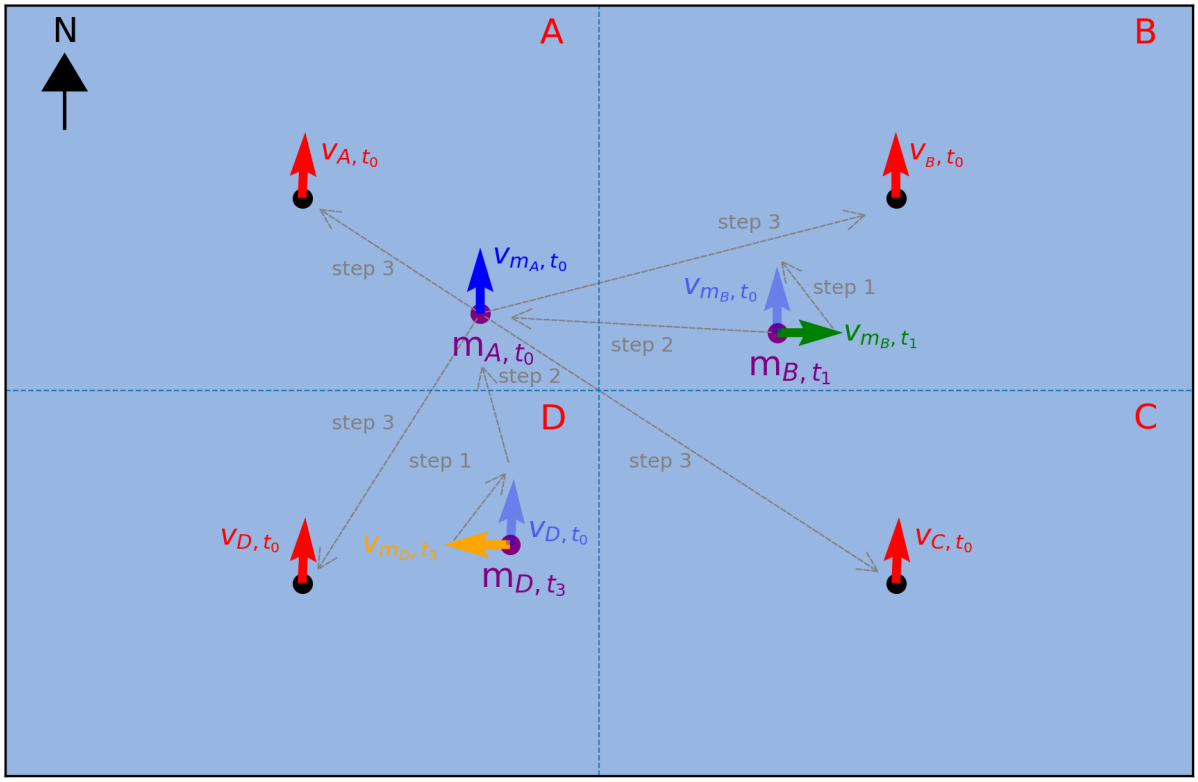

Figure 13: Schematisation showing the steps taken to get a flow velocity vector $\mathbf{v}$ for each grid cell by using the STEP method. The non-faded blue, green, and orange arrows show measured velocities at measurement locations m_A, m_B, and m_D at times t_0, t_1, and t_3 respectively. The faded blue arrows show computed predictions at measurement locations m_B and m_D at time t_0. The non-faded red arrows show the final model predictions in the middle of all grid cells at time t_0. The black arrow indicates the direction of the north.

Step 1: First, an estimation of the flow velocities at t_0 for the grid cells with measurements is needed, but at a different time. In Figure 13, this is $\mathbf{v}_{m_B,t_1}$ in grid cell B at time t_1 and $\mathbf{v}_{m_D,t_3}$ in grid cell D at t_3. From these velocities, the goal is to get an estimation for $\mathbf{v}_{m_B,t_0}$, and $\mathbf{v}_{m_D,t_0}$. This can be calculated by deconstructing it in the eastward and northward components and using Equation 4. In this case, the spatial phase differences $\Delta\phi_{j,u}$ and $\Delta\phi_{j,v}$ are 0 since the velocities at the same location are computed. Hence, the velocities only depend on the differences in time. For grid cell B this means that the phase of the tidal waves is equal to the phase at time t_1 plus the amount of tidal cycles that have taken place between t_1 and

t_0:

$$u_j(x_{m_B}, y_{m_B}, t_0) = A_{j,u} \cos\left(\phi_{j,u}(t_1) + 2\pi\sigma_j(t_1 - t_0)\right), \\ v_j(x_{m_B}, y_{m_B}, t_0) = A_{j,v} \cos\left(\phi_{j,v}(t_1) + 2\pi\sigma_j(t_1 - t_0)\right). \tag{9}$$

Step 2: This yields an estimation of the tidal flow at the measurement locations in grid cells B and D at time t_0. From this, the spatial phase difference between locations m_B and m_D and location m_A can be estimated. In this case the time difference Δt in Equation 8 is 0. Rewriting Equation 8 for grid cell B yields:

$$u_j(x_{m_B}, y_{m_B}, t_0) = A_{j,u} \cos\left(\phi_{j,u}(t_0) - \Delta\phi_{j,u,B}\right), \\ v_j(x_{m_B}, y_{m_B}, t_0) = A_{j,v} \cos\left(\phi_{j,v}(t_0) - \Delta\phi_{j,v,B}\right). \tag{10}$$

Equation 9 gives an estimation for $u_j(x_{m_B}, y_{m_B}, t_0)$ and $v_j(x_{m_B}, y_{m_B}, t_0)$. The amplitudes $A_{j,u}$ and $A_{j,v}$ are calculated using Equation 5 and $\phi_{j,u}(t_0)$ and $\phi_{j,v}(t_0)$ can be calculated using Equation 7. This means that the only unknowns in Equation 10 are the spatial phase differences $\Delta\phi_{j,u,B}$ and $\Delta\phi_{j,v,B}$. Rewriting Equation 10, yields:

$$\Delta\phi_{j,u,B} = -\cos^{-1}\left(\frac{u_j(x_{m_B}, y_{m_B}, t_0)}{A_{j,u}}\right) + \phi_{j,u}(t_0), \\ \Delta\phi_{j,v,B} = -\cos^{-1}\left(\frac{v_j(x_{m_B}, y_{m_B}, t_0)}{A_{j,v}}\right) + \phi_{j,v}(t_0). \tag{11}$$

Now, this process can be repeated for grid cell D. However, since the distance between the middle of grid cell A and grid cell B and between the middle of grid cell A and grid cell D is different, the spatial phase difference needs to be divided by the distance to get a spatial phase difference per meter:

$$\Delta\Phi_{j,u,B} = \frac{\Delta\phi_{j,u,B}}{d_{m_B}}, \\ \Delta\Phi_{j,v,B} = \frac{\Delta\phi_{j,v,B}}{d_{m_B}}, \tag{12}$$

where $d_{m_B} = \sqrt{(x_{m_B} - x_{m_A})^2 + (y_{m_B} - y_{m_A})^2}$ is the distance between the measurement location A and measurement location B.

Step 3: This yields an estimation for the spatial phase difference per meter based on the measurements in grid cells B and D. To get an average spatial phase difference, all the spatial phase differences need to be averaged. In this example, having two estimations for the spatial phase difference, this becomes:

$$\Delta\Phi_{j,u} = \frac{\Delta\Phi_{j,u,B} + \Delta\Phi_{j,u,D}}{2}, \\ \Delta\Phi_{j,v} = \frac{\Delta\Phi_{j,v,B} + \Delta\Phi_{j,v,D}}{2}. \tag{13}$$

Using this an estimation can be made for all grid cells, even the ones without measurements, at time t_0. Again, at this moment the time difference $\Delta t = 0$, meaning the velocities in the middle of each grid cell only depend on the phase at t_0 and the spatial phase difference. Using Equation 8 gives:

$$u_j(x_B, y_B, t_0) = A_{j,u} \cos\left(\phi_{j,u}(t_0) - \Delta\Phi_{j,u} d_B\right), \\ v_j(x_B, y_B, t_0) = A_{j,v} \cos\left(\phi_{j,v}(t_0) - \Delta\Phi_{j,v} d_B\right), \tag{14}$$

where $d_B = \sqrt{(x_B - x_{m_A})^2 + (y_B - y_{m_A})^2}$ is the distance between measurement location m_A and the middle of grid cell B.

These 3 steps have to be taken for each of the tidal constituents for which the signal-to-noise ratio is larger than 2.0. To get the final expression for the velocities at t_0 all expressions for the eastward and northward velocities of the significant tidal calculations as calculated in Equation 14 need to be added together, which yields that the final estimation for the tidal flow velocity in cell B becomes:

$$u(x_B, y_B, t_0) = \sum_{j, snr_j > 2.0} u_j(x_B, y_B, t_0), \\ v(x_B, y_B, t_0) = \sum_{j, snr_j > 2.0} v_j(x_B, y_B, t_0). \tag{15}$$

For each time step, a complete flow velocity field can be obtained for the model with this method.

4.3.2 Wave Celerity (WC) Method

The second approach is based on the wave celerity, which is the speed with which the tidal wave propagates. This method will be explained following two steps and is visualised in Figure 14.

Step 1: One of the assumptions that is made for method 1 to work is that the tidal velocities at time t_0 are located at the mean measurement location m_A in grid cell A. However, when performing the harmonic analysis, the assumption is made that the ship is located in one place all the time. This means that the reference location for the tidal velocities is actually the average location of the ship during the whole measurement period. This means that the output of the harmonic analysis is $u_j(x_{ref}, y_{ref}, t)$ and $v_j(x_{ref}, y_{ref}, t)$ for tidal constituent j, and for this example:

$$x_{ref} = \frac{x_{m_A} + x_{m_B} + x_{m_C} + x_{m_D}}{4}, \qquad y_{ref} = \frac{y_{m_A} + y_{m_B} + y_{m_C} + y_{m_D}}{4}. \tag{16}$$

Step 2: Using the reference location, the spatial phase difference needs to be estimated. Since the tidal wavelength, several hundred km, is much larger than the water depth, which is between 20 and 40 m in the North Sea, the assumption can be made that tidal waves behave as shallow water waves. This yields that the wave celerity $c = \sqrt{gh}$, Here g is the gravitational acceleration of 9.81 m/s^2 and h is the water depth. Since the bathymetry can change between two grid cells, this results in a wave celerity per grid cell, based on the average water depth of that grid cell. Hence, when travelling in grid cell A the wave celerity is $c_A = \sqrt{gh_A}$ and in grid cell B, the wave celerity is $c_B = \sqrt{gh_B}$.

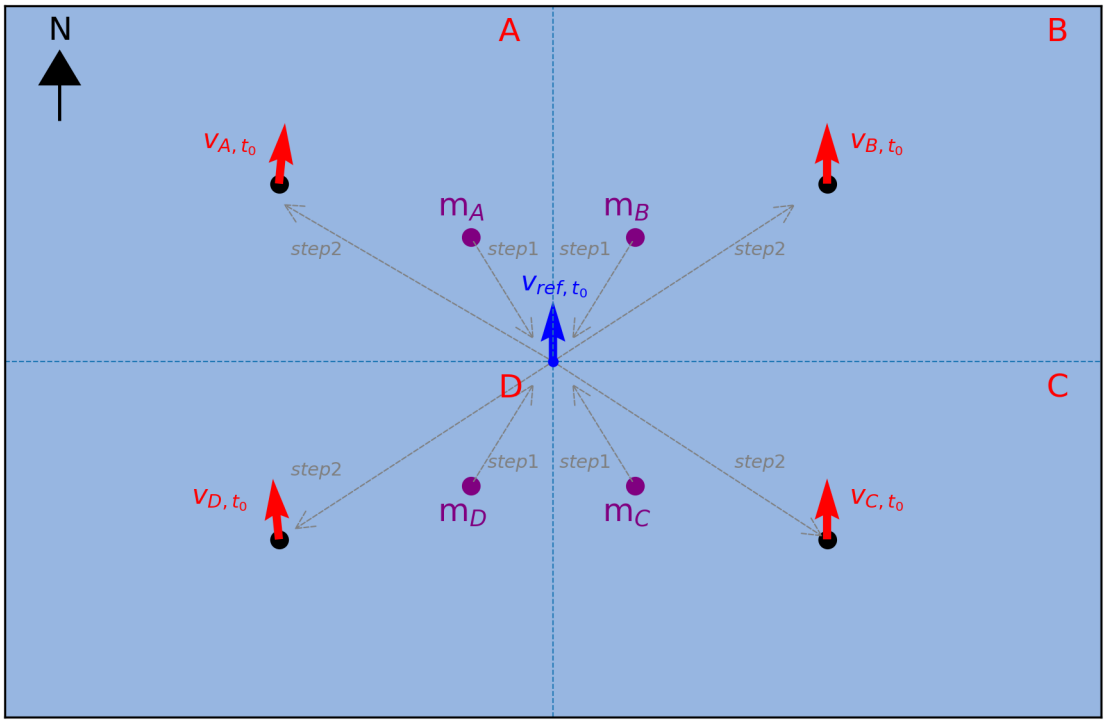

Figure 14: Schematisation showing the steps taken to get a flow velocity vector **v** in each grid cell by using the Wave Celerity Method. Here the purple dots represent the average measurement location in each grid. The blue arrow shows the reference velocity and the red arrows show the predicted tidal velocities. The black arrow indicates the direction of the north.

To get the effect of the wave celerity on the propagation of the northward and eastward tidal velocities, the wave celerity needs to be deconstructed into the north- and eastward wave celerity. This can be done by using the output of the harmonic analysis, which gives the eastward velocity $u_j(x_{ref}, y_{ref}, t)$ and northward velocity

$v_j(x_{ref}, y_{ref}, t)$. From this the group wave direction α_j can be computed for tidal constituent j:

$$\alpha_j = \tan^{-1}\left(\frac{u_{j,0}(x,y,t)}{v_{j,0}(x,y,t)}\right). \tag{17}$$

From there the eastward and northward wave celerity in grid cell B can be calculated:

$$\begin{aligned} c_{j,u,B} &= c_B \sin\alpha_j, \\ c_{j,v,B} &= c_B \cos\alpha_j. \end{aligned} \tag{18}$$

From this, the spatial phase difference between grid cells can be calculated. Using the angular frequency σ_j, which represents the number of cycles per second, the number of degrees per meter and hence the spatial phase difference per meter $\Delta\Phi_{j,u}$ and $\Delta\Phi_{j,v}$ can be calculated, for the east- and northward velocities respectively. For grid cell B this yields:

$$\begin{aligned} \Delta\Phi_{j,u,B} &= \frac{2\pi\sigma_j}{c_{j,u,B}}, \\ \Delta\Phi_{j,v,B} &= \frac{2\pi\sigma_j}{c_{j,v,B}}. \end{aligned} \tag{19}$$

Using $\Delta\Phi_{j,u,B}$ and $\Delta\Phi_{j,v,B}$ in Equation 14 gives an estimate of the tidal wave propagation in the east- and northward directions per tidal constituent. However, to get the spatial phase difference at grid cell B for this case, the phase in grid cell B should be compared to the reference location. This means that the distance to the middle of grid cell B in Equation 14 now is:

$$d_B = \sqrt{(x_B - x_{ref})^2 + (y_B - y_{ref})^2}. \tag{20}$$

To get an expression for the total tidal flow in grid cell B, the tidal waves for the significant tidal constituents need to be added together, which is shown in Equation 15.

4.4 Validation Techniques

To validate the model, several steps will be taken. First of all, it is checked whether the assumption that the amplitudes are equal in the whole model domain is valid. Next, the tidal flow velocity output of the model is compared with the results from the DCSM and buoy data from a buoy nearby.

4.4.1 Tidal Ellipse Verification

To test the assumption that the tidal ellipse parameters of each tidal constituent are the same over the whole model domain, the harmonic analysis needs to be performed again. For each of the grid cells in the model domain, a time series of the northward and eastward velocities at the middle of each grid cell is computed for both methods. Applying the harmonic analysis to these new time series will yield a new estimation of the tidal ellipse, the phase, the angular frequency, and the signal-to-noise ratio of each of the considered tidal constituents, but now for each grid cell. To see if this assumption was valid, these values are then compared to the assumed values for the entire model domain.

4.4.2 Other Velocity Data Sources

To validate the output of both methods, it is compared to the output of two other sources recording flow velocity data.

Dutch Coastal Shelf Model:
First of all, the DCSM, which has been introduced in Section 1, is compared to the developed model. To do this, the DCSM will be run for the same model domain, by assigning multiple observation points in the model domain. The DCSM has been run as a 2DH model, only using the tidal forcings as input. Hence, this yields as output the depth-averaged tidal velocities at each of the observation points. The DCSM simulation is started a few days early so that the warm-up period of the DCSM is included.

To compare the results of the DCSM to the output of our model, the developed model is run with a grid so that each observation point coincides with the middle of a grid cell. The STEP and WC method

both give depth-averaged velocities as output, which can be used for the comparison The two outputs at each observation point will then be compared based on the cross-correlation to see if the behaviour of the time series of time is correlated. This is done by checking the cross-correlation at lag 0 since ideally, the results should be identical and hence no lag should be present between the time series. Doing this for each observation point gives an average cross-correlation between the results of the model and the DCSM. The cross-correlation will be calculated for both tidal propagation methods implemented in the models. A cross-correlation of 1 indicates a perfect correlation between the two time series, 0 means no correlation and -1 means an inverse correlation (Bourke, 1996).

To check the quantitative output of the STEP and WC method, the RMSD (Root-Mean-Squared Deviation) is calculated, which shows the difference between the predicted value of the STEP and WC method with the value predicted by the DCSM. A low score implies a smaller difference between the time series, while a higher score implies a large difference between the values in the two time series (Hodson, 2022).

Buoy Data:
To compare the model with buoy data, a buoy near the model domain is considered. The closest buoy with flow velocity measurements near the model domain is the buoy near IJmuiden at 80 km distance. The location of the buoy is shown in Figure 3. Since the buoy only records the flow velocities at the water surface, the buoy measurements are compared with the output of both methods when applied to the uppermost layer of the DVL measurements. These measurements are not made at the water surface, but at 3 m below the draft of the ship, so that the measurements are not affected by the ship sailing. Since the model currently does not contain all processes affecting the flow velocities, it is only interesting to compare the tidal flow velocities with the buoy. Based on the two tidal propagation formulas discussed before, the model can yield a prediction of the tidal velocities at the location of the buoy. To get only the tidal velocities from the buoy measurements, a harmonic analysis needs to be applied to the buoy data. The output of this harmonic analysis can then be used to compare the tidal ellipse, frequency, and phase between the model and the buoy measurements. Also, the cross-correlation and RMSD between the buoy measurements and the model output will be compared.

5 Results

Here, the several steps to develop the model, which are described in Section 4, are applied to the data provided by The Netherlands Hydrographic Service. First, the tidal signal will be extracted, after which the output of the model for both the STEP and WC method will be shown.

5.1 Tidal Signal

The velocity time series can be deconstructed into a tidal signal and a residual signal. To get the tidal signal, a harmonic analysis is performed on the time series for the north- and eastward component of the velocity, according to the procedure described in Section 4.1. In Figures 15 and 16, the original filtered time series used as input for the harmonic analysis, the constructed tidal signal, and the residual signal for the eastward and northward velocity, respectively, can be seen for the top part of the water column. The output of the harmonic analysis showed that the significant tidal constituents for the top part of the water column are the M2, M3, M4, 2MK5, M6, and M8 tides. This means that of the considered tides in the harmonic analysis, only the K1 tide and 3MK7 are not significant in the top part of the water column. The dominant tidal constituent in the North Sea is the M2 tide (Walters, 1987), which is included in the output. However, other important tidal constituents, such as the O1, S2, K2 and N2 tides are not included in the model. This can be explained by the fact that the input time series only spans 5 days, causing some tidal constituents to not be included in the harmonic analysis, since for this a time series of 18.6 years is needed. The ellipse parameters that came out of the harmonic analysis can be found in Table 9 in Appendix A.2.

For the bottom part of the water column, the input, tidal, and residual signal from the harmonic analysis can be seen in Figures 17 and 18. Comparing this to the top part of the water column, it can be seen that the tidal signal in the bottom part is less present. These differences can be explained by the fact that the observations for the bottom part of the water column show a less obvious periodic behaviour, which means the tidal signal is not clearly present, making the results of the harmonic analysis in the bottom part of the water column less strong. This can be caused by the fact that in the filtering process, more data is filtered out in the bottom of the water column due to being close to the sea bed, meaning that the harmonic analysis is performed on less data. Furthermore, in the bottom layer of the water column, the flow velocity is more influenced by the interaction with the sea bed, causing bottom friction and turbulence, making it more

difficult to extract the tidal signal. The harmonic analysis showed that the significant tidal constituents for the bottom part of the water column are the M2 and 2MK5 tides. For the other significant constituents in the top part of the water column, it can be seen that those are still higher compared to the K1 and 3MK7 constituents, but just below the signal-to-noise ratio of 2.0. Comparing the phase and major axis of these tidal constituents for the top and bottom layer of the water column, it can be seen that for the start of this time period, the phase of the M2 tides and 2MK5 tides in the top layer of the water column is 60.74° and 343.54°, respectively. In the bottom layer of the water column, these phases are 63.28° and 202.82°. This difference can be explained by stratification and inertia differences between the two layers of the water column (Maas and Van Haren, 1987). Looking at the major axis of the tidal ellipse, the value for the M2 tide is 0.74 m/s and for the M6 tide is 0.18 m/s for the top layer of the water column. For the bottom layer of the water column, this is 0.18 m/s and 0.019 m/s for the M2 tide and 2MK5 tide respectively. These differences can again be explained by the fact that the tidal behaviour is less visible in the observations for the bottom part of the water column. The complete output of the harmonic analysis for the bottom part of the water column can be seen in Table 10.

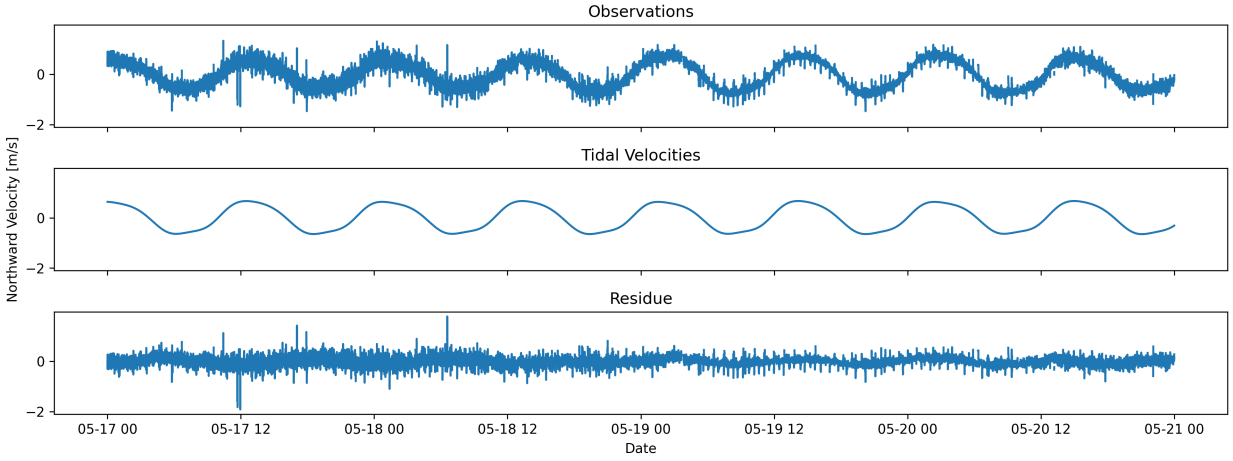

Figure 15: Input and output of the harmonic analysis for the top part of the water column for the northward velocities.

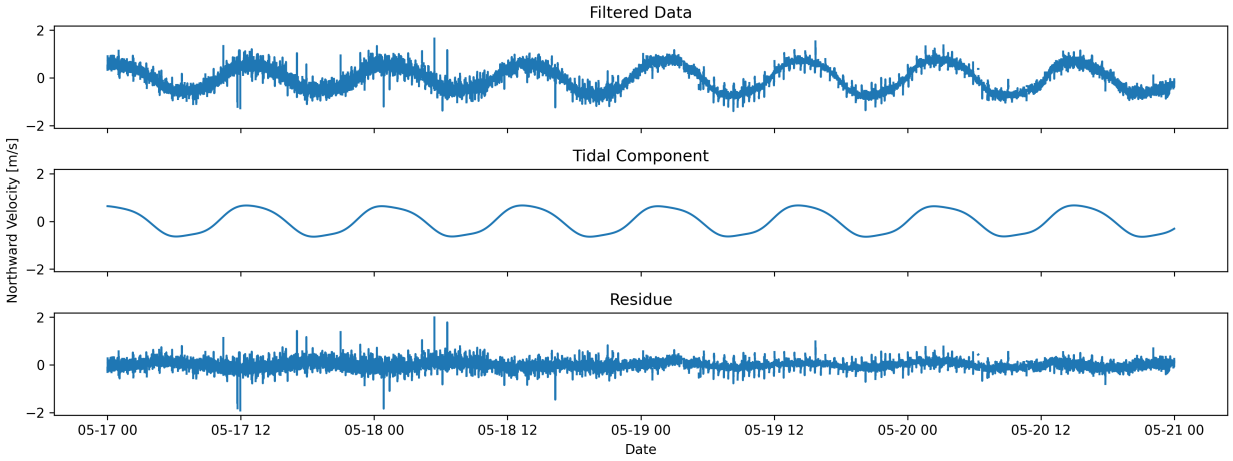

Figure 16: Input and output of the harmonic analysis for the top part of the water column for the eastward velocities.

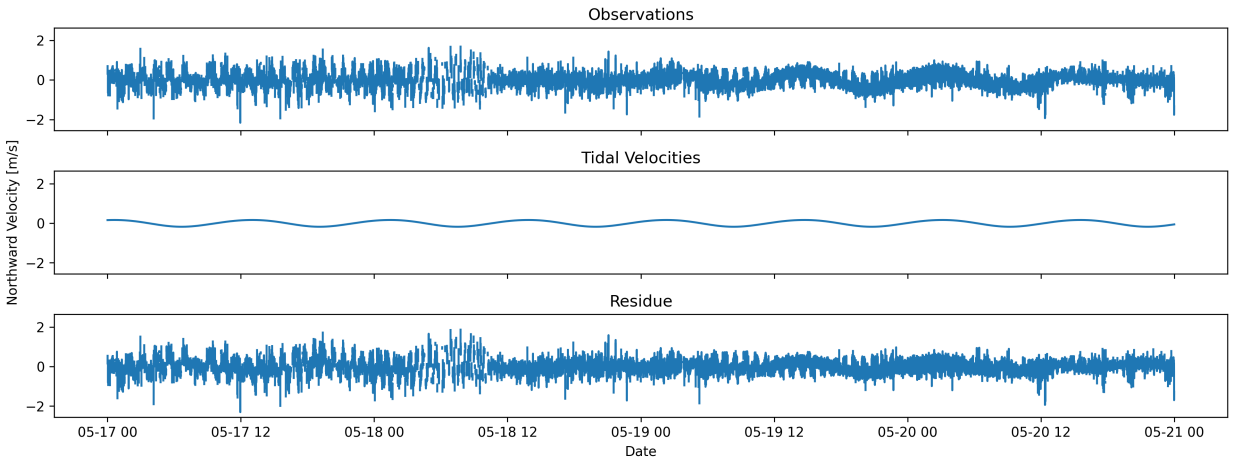

Figure 17: Input and output of the harmonic analysis for the bottom part of the water column for the northward velocities.

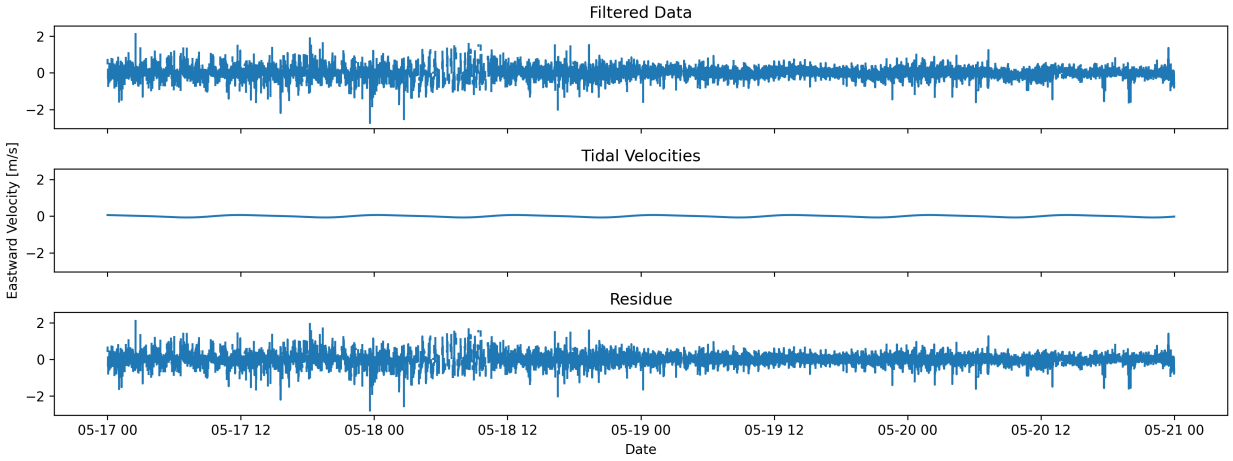

Figure 18: Input and output of the harmonic analysis for the bottom part of the water column for the eastward velocities.

5.2 Model Output

For the two developed methods to estimate the spatial phase difference, the different model outputs are discussed below. First, the output of the STEP method will be discussed, after which the WC method will be discussed. Finally, a comparison between both methods will be made.

5.2.1 STEP method

For the predictions made by the STEP method, it is interesting to look at the spatial output for three different moments in the tidal cycle, the moment where the north and eastward tidal velocity is highest, the moment where it is the lowest and the moment where the direction of the tidal wave is changing. This can be seen in Figures 19, 20 and 21. In these figures, the velocity vector is plotted for each grid cell. Here, it can be seen that the direction and magnitude can differ largely between each grid cell and that this behaviour is present for each of the different moments in the tidal cycle.

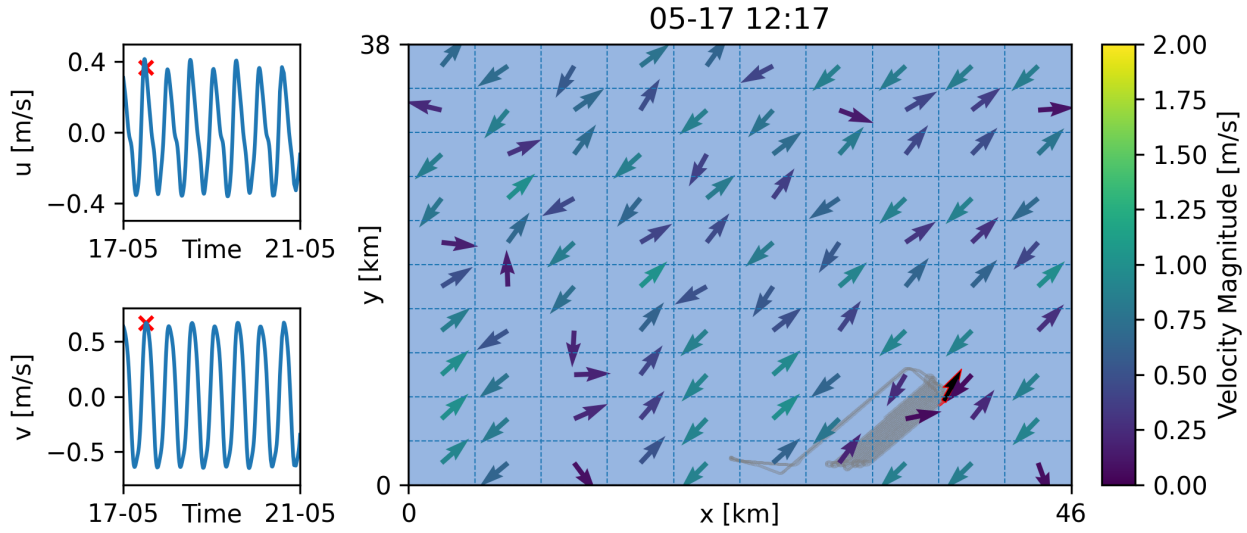

Figure 19: The predicted tidal velocities for the STEP method for maximum eastward and northward velocities. The east and northward velocities are plotted in the left two plots, computed from the harmonic analysis. In these time series, the moment in the tidal cycle is indicated with a red cross. In the right plot, the red line indicates the measurements made around the time shown in the figure, the arrow with a red contour the reference velocity based on these measurements and the grey lines are old measurement locations.

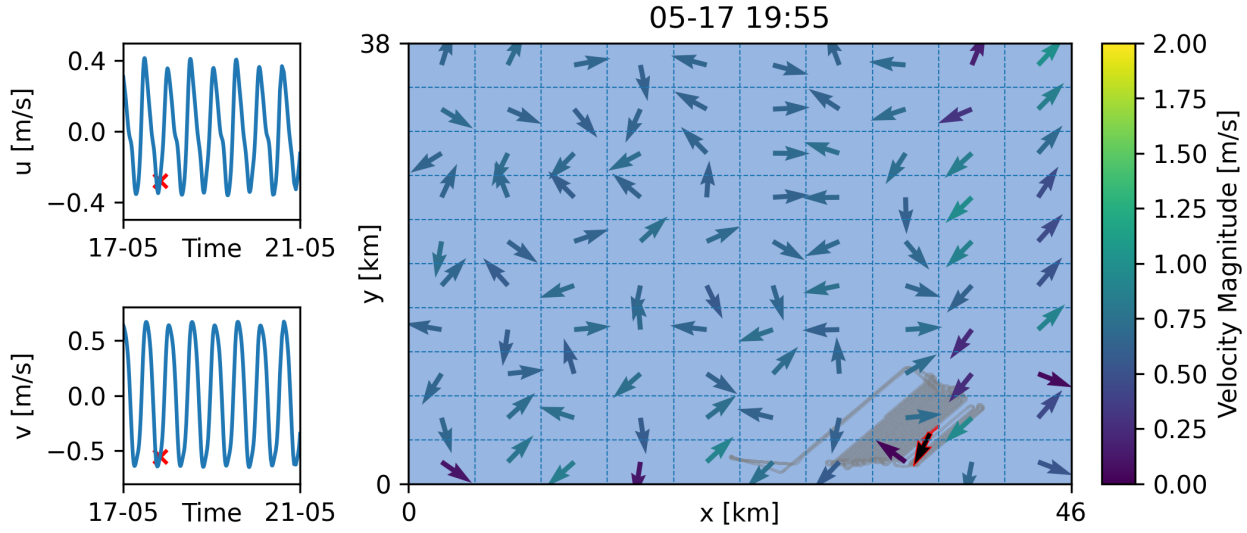

Figure 20: The predicted tidal velocities for the STEP method for minimum eastward and northward velocities. The east and northward velocities are plotted in the left two plots, computed from the harmonic analysis. In these time series, the moment in the tidal cycle is indicated with a red cross. In the right plot, the red line indicates the measurements made around the time shown in the figure, the arrow with red contour the reference velocity based on these measurements and the grey lines are old measurement locations.

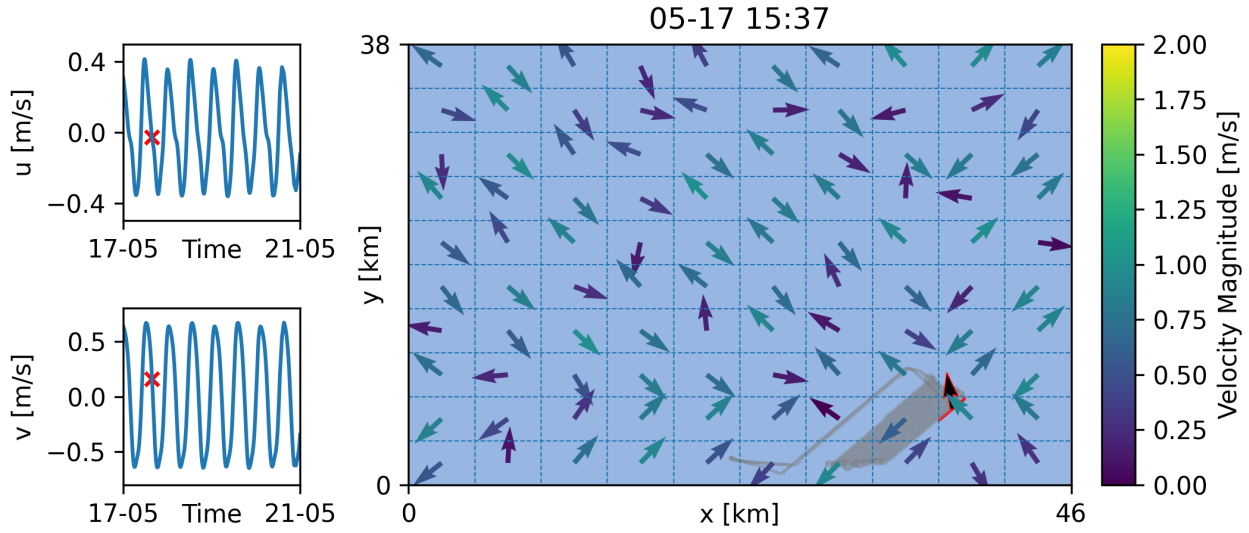

Figure 21: The predicted tidal velocities for the STEP method when the direction of the tide is changing. The east and northward velocities are plotted in the left two plots, computed from the harmonic analysis. In these time series, the moment in the tidal cycle is indicated with a red cross. In the right plot, the red line indicates the measurements made around the time shown in the figure, the arrow with red contour the reference velocity based on these measurements and the grey lines are old measurement locations.

Furthermore, it is interesting to look at the temporal output for the STEP method. In Figures 22 and 23 the predicted and measured eastward and northward velocities can be shown. These figures show that first of all, the uncertainty in the predicted velocities is high, meaning that the predictions are inaccurate. Especially when looking at the predictions at the average measurement location, it can be seen that the variation over time in both the eastward and northward velocity is much larger for the predictions, showing that not only over distance but also over time the variation in the magnitude and direction of the velocity vector is larger than for the measurements. What can also be seen, is that at the start of the time period, the variation in the direction and magnitude is similar to the measurements. Later on in the time series, the predictions will show a larger variation in the magnitude in direction, indicating that the difference in phase for the predictions and measurements develops over time. Looking at the amplitudes of the predicted and measured time series, it can be seen that for the eastward velocities the predicted amplitudes are twice as large as the measured velocities, while the amplitude for the northwards velocities are similar. This indicates that the estimated amplitudes from the tidal ellipse are in the correct order of magnitude for the northward velocities, but not for the eastward velocities.

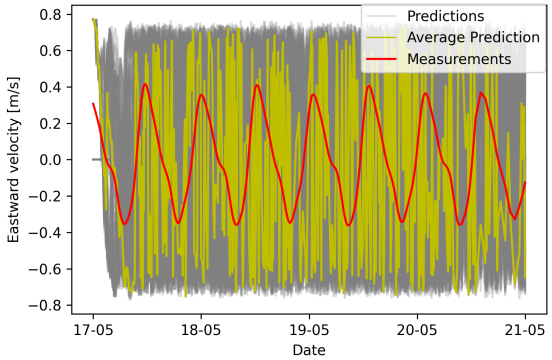

Figure 22: Predicted and measured eastward velocities in the model domain for the STEP method. For each of the grid cells in the model domain, the predicted eastward velocities are plotted in grey. The yellow line shows the predicted velocities at the average measurement location.

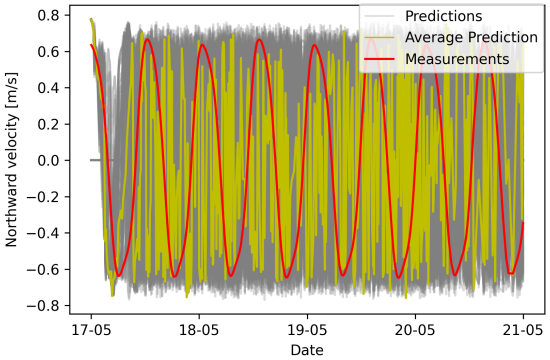

Figure 23: Predicted and measured northward velocities in the model domain for the STEP method. For each of the grid cells in the model domain, the predicted eastward velocities are plotted in grey. The yellow line shows the predicted velocities at the average measurement location.

In the STEP method, the spatial phase difference is calculated for each time step, meaning that over time there will differences in the spatial phase difference. Hence, looking at the spatial phase difference over the model domain for the M2-tidal wave, shown in Figures 24, 25, 26 and 27, it can be seen that at the start of the time period, the spatial phase difference is between -1° and 1° compared to the reference location, for both the northward and eastward velocities. However, later in the tidal time series, this difference is between -11459° and 11459° for the eastward velocities and between -17189° and 17819° for the northward velocities. This again shows that the phase difference grows over time. Furthermore, it can be seen that in the model domain, as expected, the spatial phase difference grows when going further from the average measurement location in that grid cell, indicated by the black arrow.

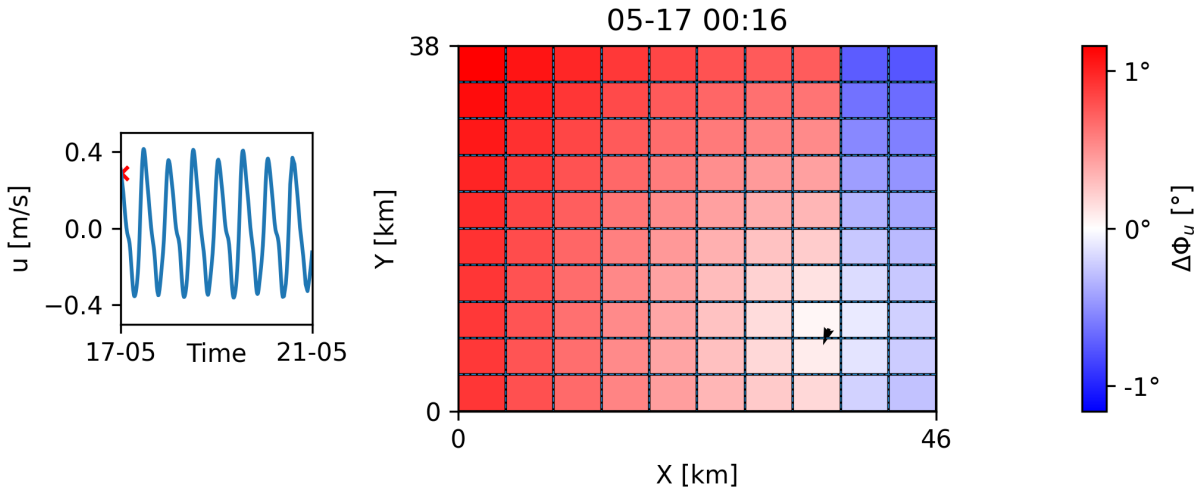

Figure 24: Predicted eastward spatial phase difference for the M2 wave for the STEP method at the start of the time series. The left plots show the moment in the tidal cycle for the eastward velocities. The black arrow shows the velocity vector at the measurement location at this moment in time.

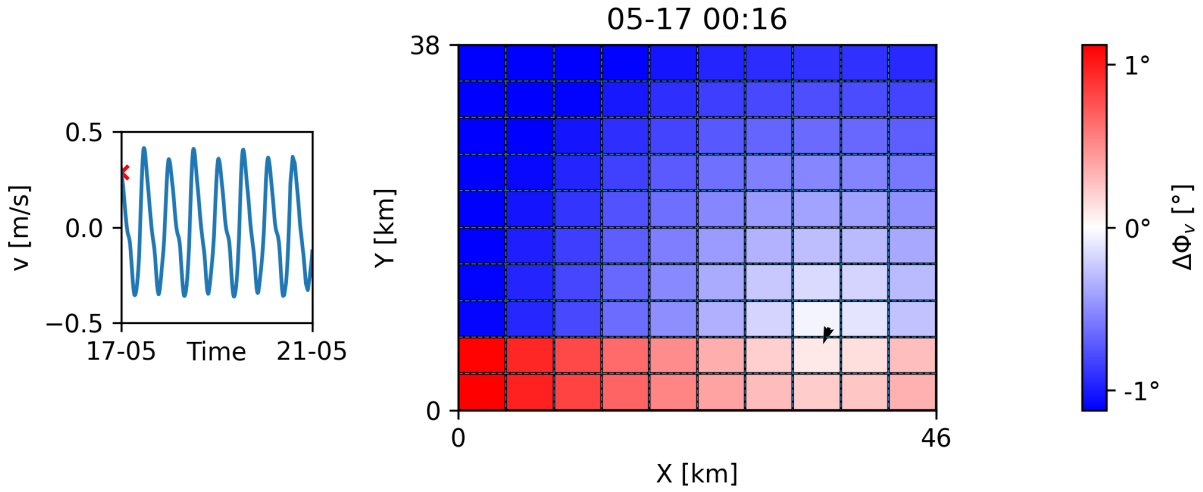

Figure 25: Predicted northward spatial phase difference for the M2 wave for the STEP method at the start of the time series. The left plot shows the moment in the tidal cycle for the northward velocities. The black arrow shows the velocity vector at the measurement location at this moment in time.

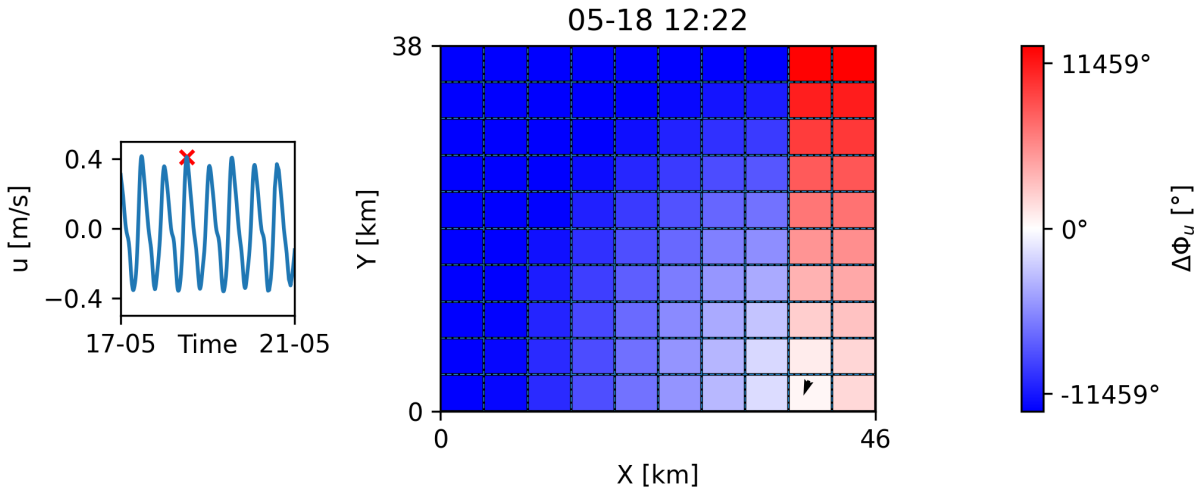

Figure 26: Predicted eastward spatial phase difference for the M2 wave for the STEP method in the middle of the time series. The left plot shows the moment in the tidal cycle for the eastward velocities. The black arrow shows the velocity vector at the measurement location at this moment in time.

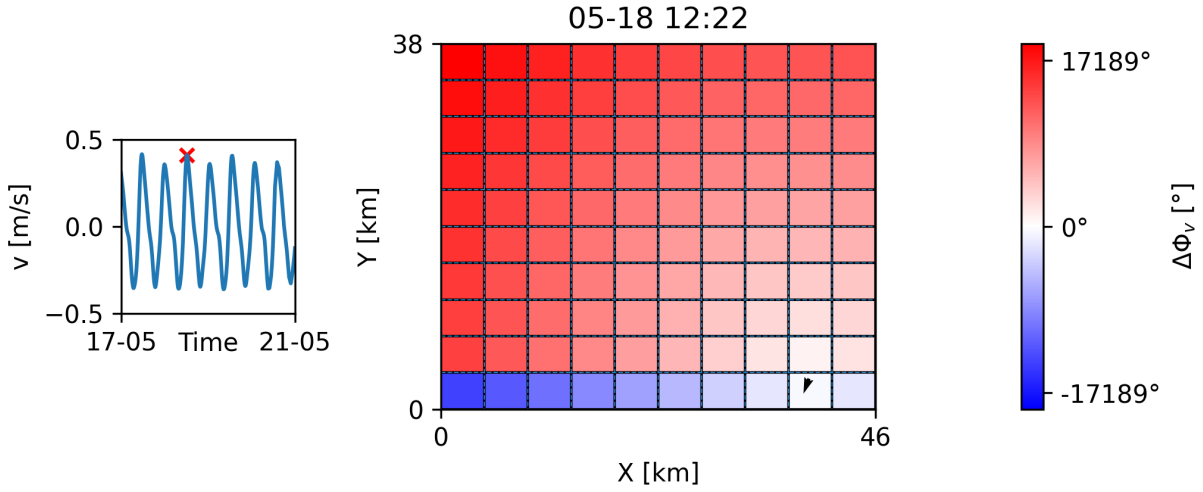

Figure 27: Predicted northward spatial phase difference for the M2 wave for the STEP method in the middle of the time series. The left plot shows the moment in the tidal cycle for the northward velocities. The black arrow shows the velocity vector at the measurement location at this moment in time.

5.2.2 WC method

For the WC method, the same moments in the tidal cycle are considered as for the STEP method, shown in Figures 28, 29 and 30. In Figures 28 and 29, it can be seen that there is not much variation in the direction of the velocities and the magnitude of the velocities within the model domain. Compared to the velocity at the reference location, it can be seen that the magnitude of the velocity is different, and that the eastward component in the velocity is more dominant. Looking at a moment where the tide is turning in Figure 30, it can be seen that the predicted velocities turn around earlier compared to the reference velocity. One possible cause of this is that the velocity magnitude at this moment is close to zero, hence only a slight deviation in the northward or eastward velocity from the reference velocity already shows a different direction. Also, it can be seen that the left of the reference velocity the velocities turn around counterclockwise, while on the right of the reference velocity and the the tide turns around clockwise. In reality, the tide in the Northern Hemisphere turns around counterclockwise due to the Coriolis effect (Persson, 2005). Hence, the way the tides are turning is not correctly predicted in this method.

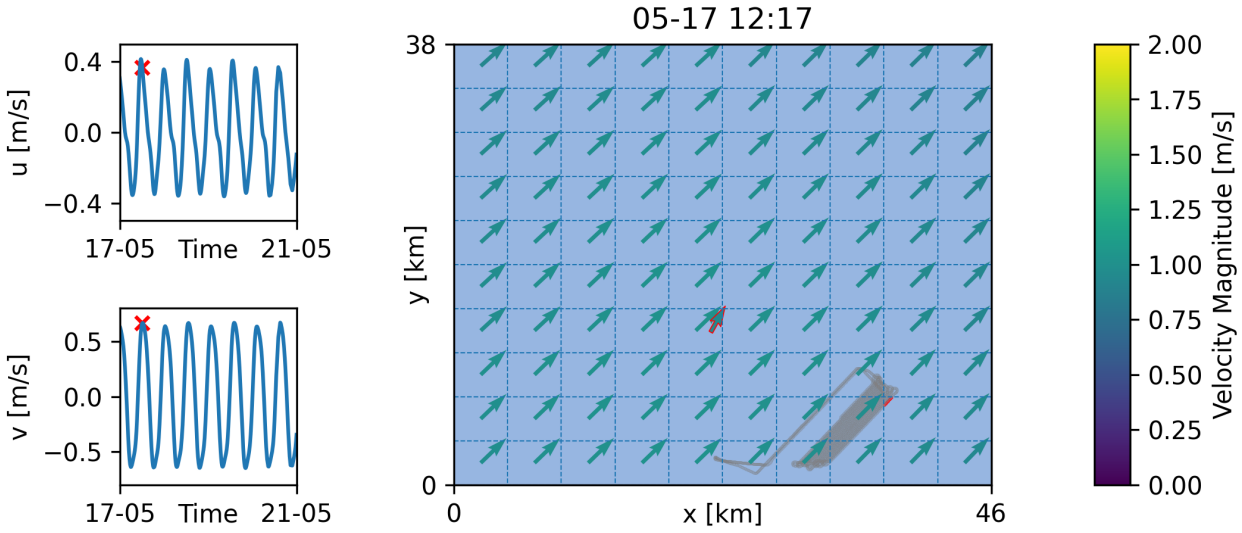

Figure 28: The predicted tidal velocities for the WC method for maximum eastward and northward velocities. The east and northward velocities are plotted in the left two plots, computed from the harmonic analysis. In these time series, the moment in the tidal cycle is indicated with a red cross In the right plot, the red line indicates the measurements made around the time shown in the figure, and the grey lines are old measurement locations. The arrow with the red contour is the velocity vector at the reference location.

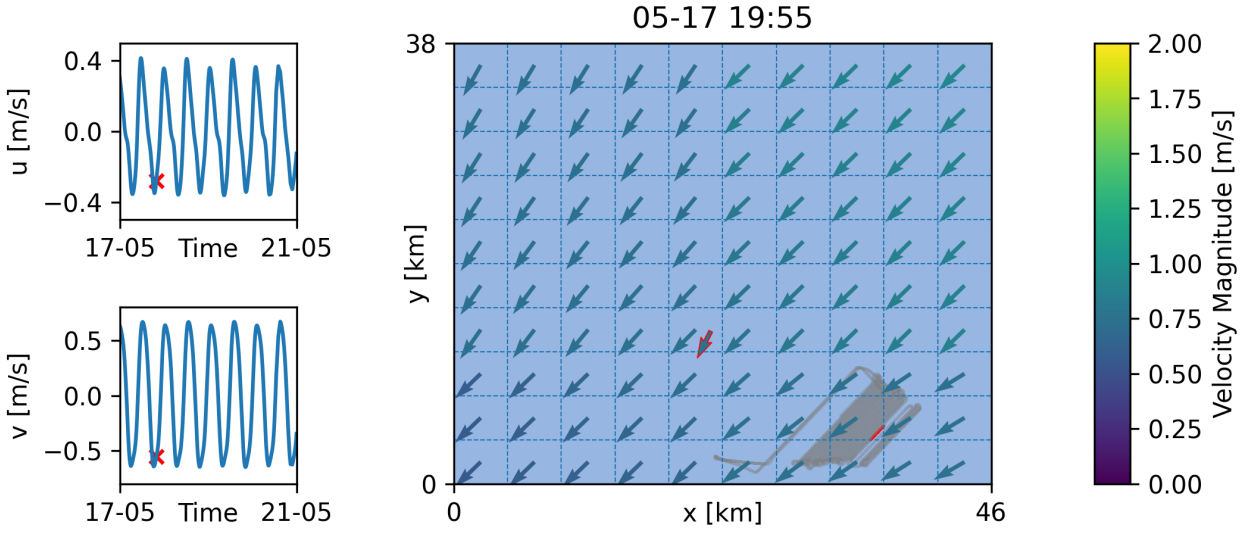

Figure 29: The predicted tidal velocities for the WC method for minimum eastward and northward velocities. The east and northward velocities are plotted in the left two plots, computed from the harmonic analysis. In these time series, the moment in the tidal cycle is indicated with a red cross. In the right plot, the red line indicates the measurements made around the time shown in the figure, and the grey lines are old measurement locations. The arrow with the red contour is the velocity vector at the reference location.

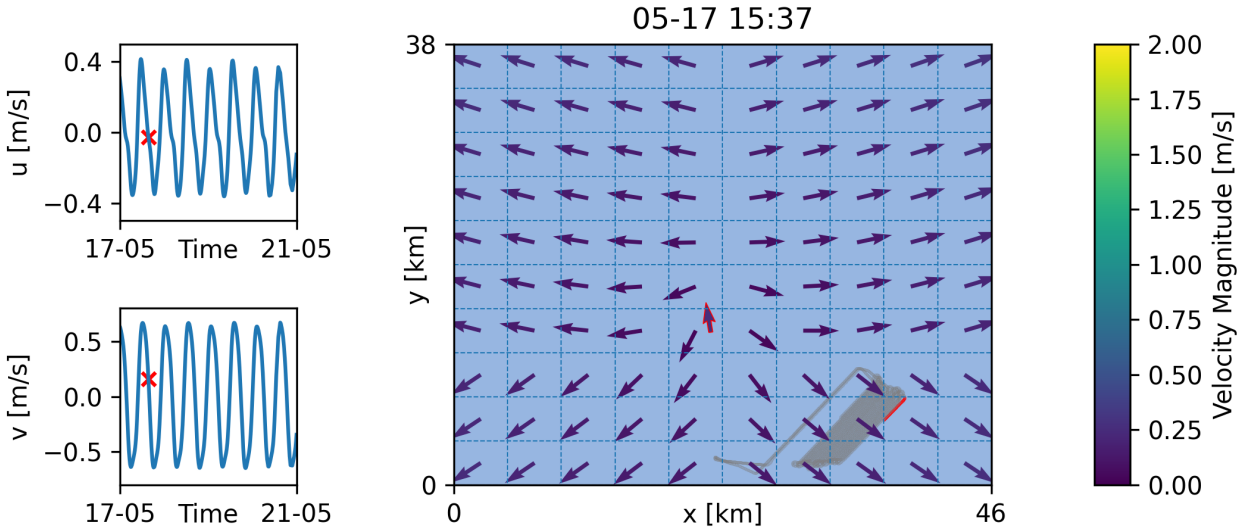

Figure 30: The predicted tidal velocities for the WC method when the direction of the tide is changing. The east and northward velocities are plotted in the left two plots, computed from the harmonic analysis. In these time series, the moment in the tidal cycle is indicated with a red cross. In the right plot, the red line indicates the measurements made around the time shown in the figure, and the grey lines are old measurement locations. The arrow with the red contour is the velocity vector at the reference location.

Looking at the temporal output from the WC method, shown in Figures 31 and 32, it can be seen that there is less variation in the predicted velocities compared to the STEP method. Comparing the predictions to the measured velocities it can be seen that the period of the predicted eastward and northward velocities is similar to the measured velocities. Again, just as for the STEP method, the amplitude of the northward velocity is similar between the predictions and the measurements and for the eastward velocity the predicted velocity are twice as high compared to the measurements. This also explains the fact that in the spatial output in Figures 28 and 29 the eastward velocity is more dominant compared to the reference velocity. In the predicted time series there are also peaks present around the times the tides are changing. This can be explained that at the moments the tides are changing there is a large spatial difference in the direction of the tides and hence in the eastward and northward velocities.

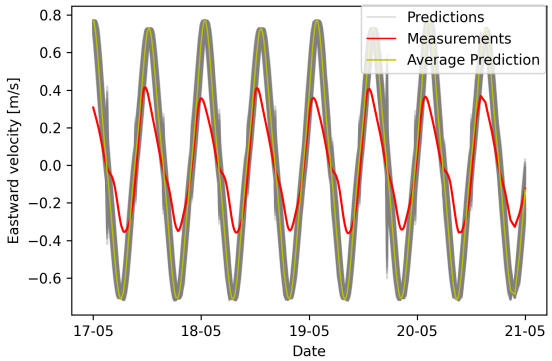

Figure 31: Predicted and measured eastward velocities in the model domain for the WC method. For each of the grid cells in the model domain, the predicted eastward velocities are plotted in grey. The yellow line shows the predicted velocities at the average measurement location.

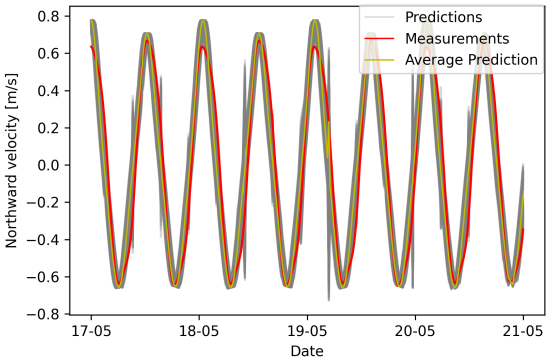

Figure 32: Predicted and measured northward velocities in the model domain for the WC method. For each of the grid cells in the model domain, the predicted northward velocities are plotted in grey. The yellow line shows the predicted velocities at the average measurement location.

Looking at the spatial phase difference for the M2 wave, shown in Figures 33 and 34, it can be seen that for both the eastward and northward velocity the spatial phase difference is between -20 and 20° compared to the reference location. Since for the WC method the spatial phase difference is indifferent to the time

step, this spatial difference is constant over time. However, the spatial phase difference in the WC method is dependent on the wave celerity $c = \sqrt{gh}$ and hence dependent on the depth of the sea bed. In Figures 35 and 36, it can be seen that there is quite some variation between the depth and hence the group speed. However, looking at the spatial phase difference this pattern is not visible. This indicates that the spatial phase difference is more dependent on the distance between each grid cell than on the depth of the sea bed in each grid cell.

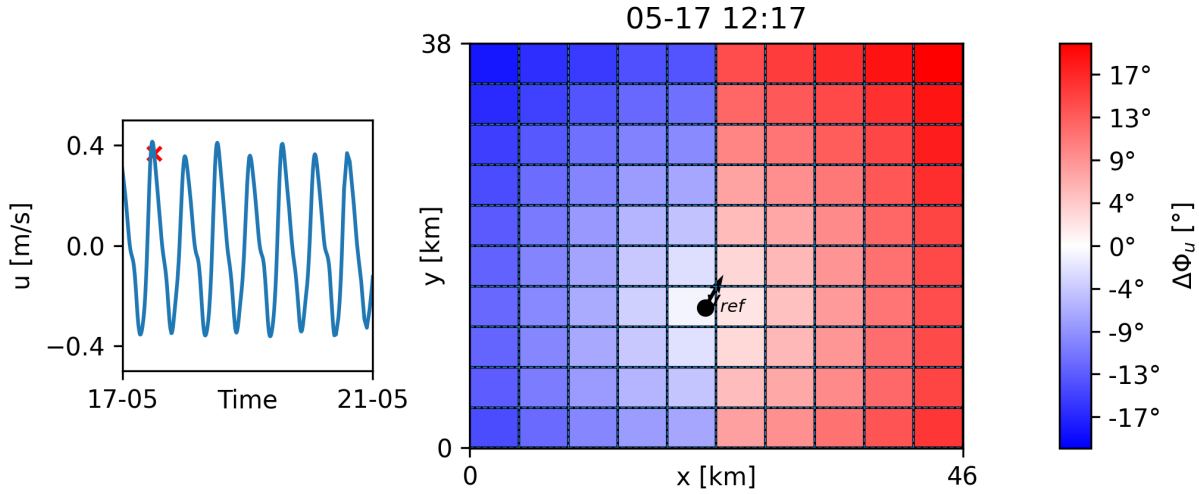

Figure 33: Predicted eastward spatial phase difference for the M2 wave for the WC method. The left plot shows the moment in the tidal cycle for the eastward velocities. The black arrow shows the velocity vector at the measurement location at this moment in time.

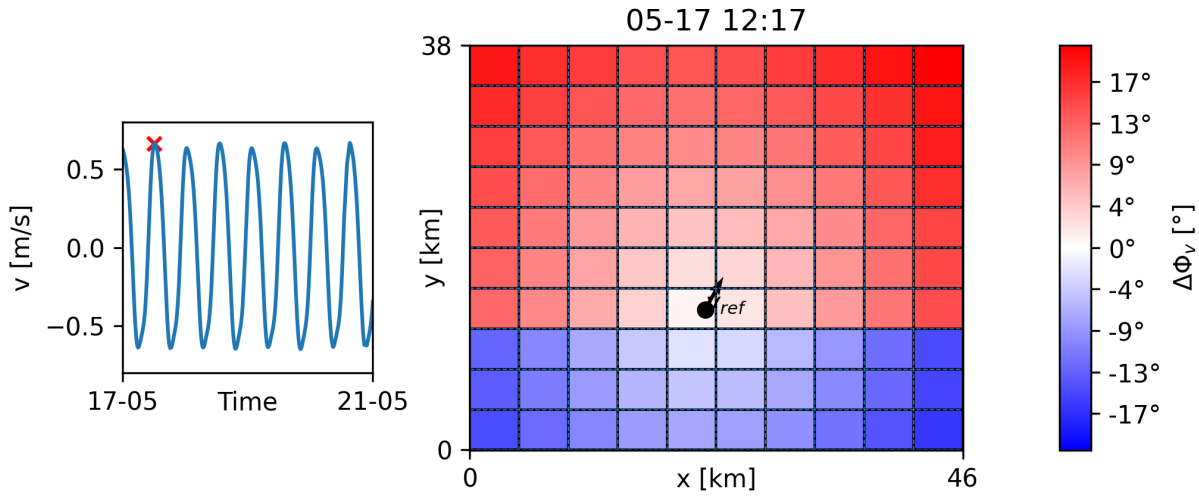

Figure 34: Predicted northward spatial phase difference for the M2 wave for the WC method. The left plot shows the moment in the tidal cycle for the northward velocities. The black arrow shows the velocity vector at the measurement location at this moment in time.

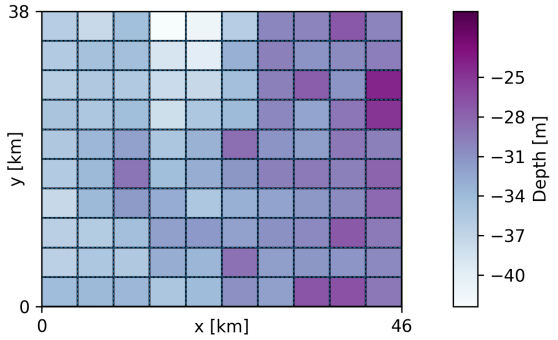

Figure 35: Average depth of each grid cell.

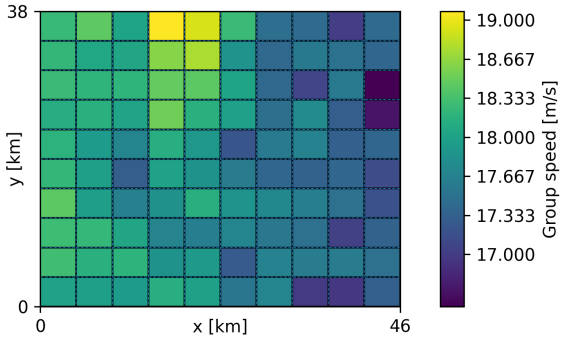

Figure 36: Average group speed in each grid cell.

To show that this model will still work for another grid cell size, the grid cells are made twice as small. The spatial output for the model can then be seen in Figure 37. Comparing this to the output at the same moment in the tidal cycle for a larger grid cell size in Figure 29, it can be seen that the output is similar and hence independent of the size of the grid. Looking at the spatial phase difference for a finer grid, shown in Figures 38 and 39, it can be seen that the variation in the spatial phase difference in the model domain, compared to the reference velocity, is again between -20° and 20°, just as for the coarser grid, shown in Figures 33 and 34. Also, comparing the pattern of the spatial phase difference in the grid, it can be seen that this is similar. Hence, this indicates that the model output remains similar for a smaller cell size.

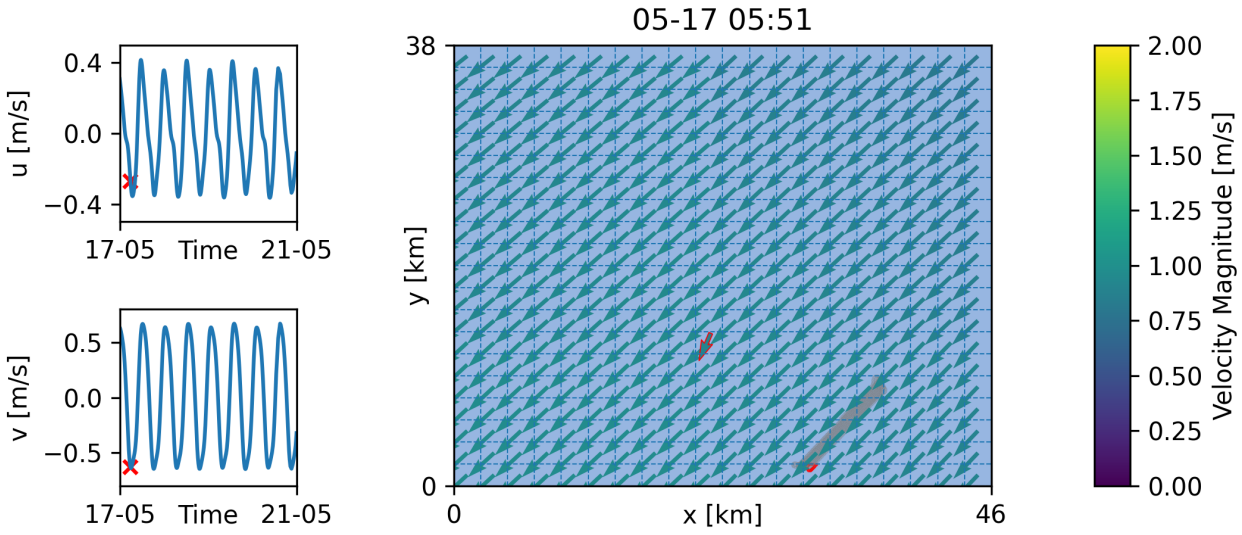

Figure 37: The predicted tidal velocities for the WC method when the direction of the tide is changing. In the two left plots, the moment in the tidal cycle is indicated with a red cross. In the right plot, the red line indicates the measurements made around the time shown in the figure, and the grey lines are old measurement locations. The arrow with the red contour is the velocity vector at the reference location.

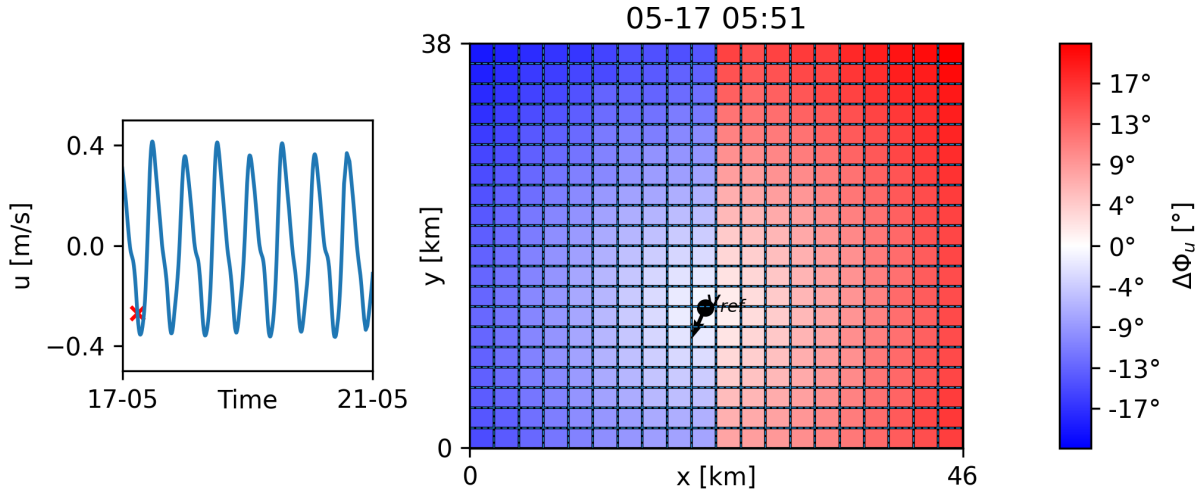

Figure 38: Predicted eastward spatial phase difference for the M2 wave for the WC method and a smaller grid size. The left plot shows the moment in the tidal cycle for the eastward velocities. The black arrow shows the velocity vector at the measurement location at this moment in time.

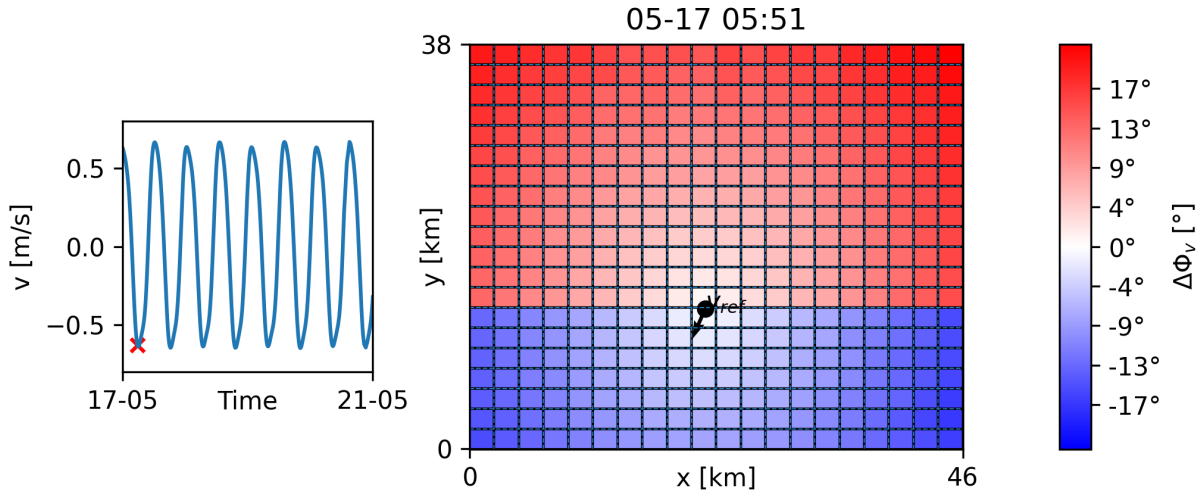

Figure 39: Predicted northward spatial phase difference for the M2 wave for the WC method and a smaller grid size. The left plot shows the moment in the tidal cycle for the northward velocities. The black arrow shows the velocity vector at the measurement location at this moment in time.

Finally, directly comparing both the methods, shown in Figure 40, directly shows the difference made in the predictions by the STEP method. In this figure, it can be seen that the flow velocity magnitudes are similar for both methods, but the directions differ quite a lot. While for the WC method the direction shows little variation over the model domain, the direction for the STEP method can change between every grid cell.

All in all, for both the STEP and WC methods, the amplitude for the northward velocity is similar to that of the measurements in each grid cell. However, for the eastward velocity, the amplitude is twice as large. Furthermore, for the STEP method, the frequency of the eastward and northward velocity waves is way larger than for the measurements, while in the WC method, this is similar. Finally, for the WC method, the spatial phase difference is mainly dependent on the distance of the grid cell to the reference location and not on the depth of the seabed in that grid cell.

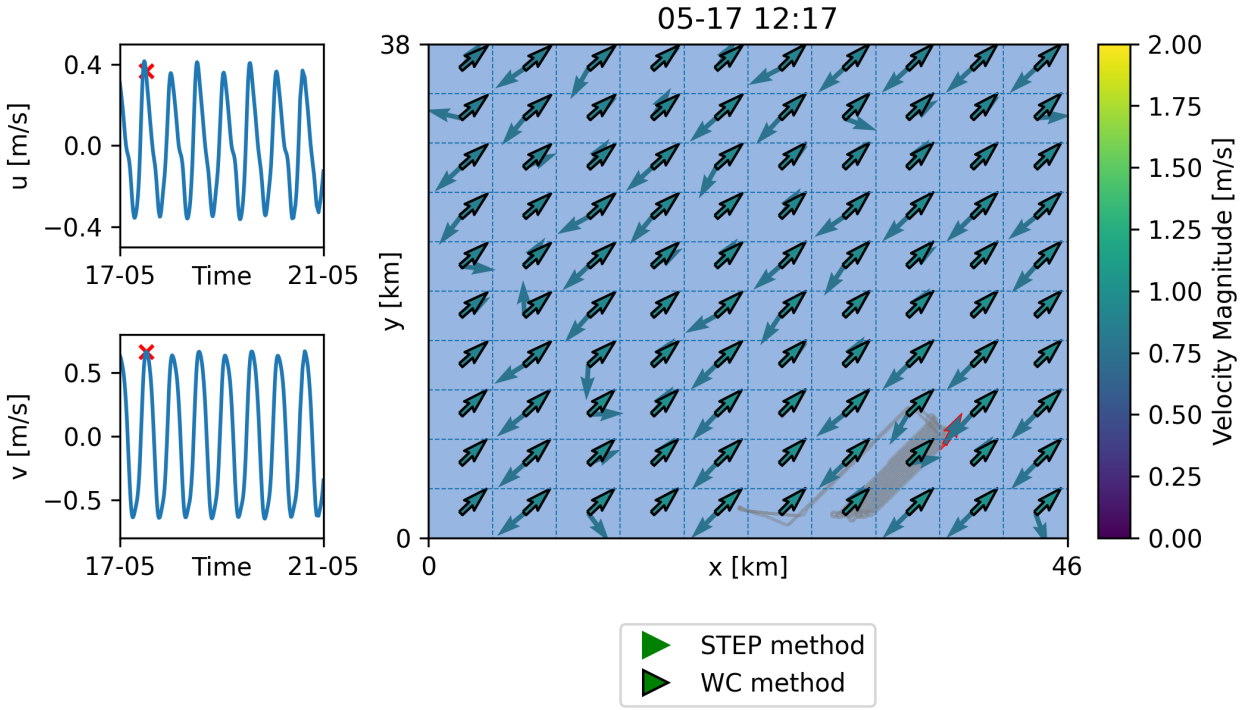

Figure 40: The predicted tidal velocities for both the STEP method and the WC method for maximum eastward and northward velocities. In the two left plots, the moment in the tidal cycle is indicated with a red cross. In the right plot, the red line indicates the measurements made around the time shown in the figure, the arrow with red contour the reference velocity based on these measurements and the grey lines are old measurement locations.

6 Validation

6.1 Tidal Ellipse Parameter Verification

In the model simulation, the assumption is made that the ellipse parameters are constant over the whole model domain. The ellipse parameters used in the model simulation for the top part of the water column are shown in Table 2.

Table 2: Output of the original harmonic analysis for the top part of the water column.

Tide	Signal-to-noise ratio	Major [m/s]	Minor [m/s]	Inclination [°]	Phase [°]
K1	0.59	0.041	-0.011	75	43
M2	$1.4 \cdot 10^2$	0.74	0.058	64	61
M3	5.2	0.085	0.010	4	23
M4	95	0.085	0.010	4	24
2MK5	4.8	0.018	-0.00010	158	344
M6	$1.8 \cdot 10^2$	0.061	-0.0081	79	53
3MK7	0.18	0.0032	0.00040	66	338
M8	4.2	0.21	-0.0043	18	21

To test whether the propagation is correct the velocity time series based on both the STEP and the WC method is saved for each grid cell, for a grid of 100 grid cells. For each of the time series, the harmonic analysis is performed, and from this, a mean value and standard deviation value for the output of the harmonic analysis are computed for the entire grid. For the STEP method, the results can be seen in Table 3. Comparing Tables 2 and 3 shows large variation in the outcome of the harmonic analysis. The signal-to-noise ratio is much smaller, indicating that the constructed tidal signals are less strong and only the M2 and M3 constituents are significant in the new time series. Furthermore, a large difference in the ellipse parameters is visible. From this, the original harmonic analysis can not be repeated. This is likely because the spatial phase difference for this method is too large and because the predicted time series does not match

the measurements, as can be seen in Figures 22 and 23 .

Table 3: Mean variables and standard values for applying harmonic analysis for each of the grid cells after applying the STEP method.

Tide	Signal-to-noise ratio		Major [m/s]		Minor [m/s]		Inclination [°]		Phase [°]	
	Mean	Std	Mean	Std	Mean	Std	Mean	Std	Mean	Std
K1	1.55	2.81	0.15	0.061	0.0043	0.035	97	75	194	10
M2	2.55	4.34	0.15	0.061	-0.033	0.036	143	61	280	9
M3	2.00	3.48	0.010	0.031	-0.0030	0.040	76	46	116	7
M4	1.11	1.41	0.071	0.022	-0.0022	0.022	99	47	179	29
2MK5	1.68	2.75	0.057	0.020	0.0078	0.021	87	48	204	36
M6	1.40	2.16	0.054	0.023	0.0025	0.018	92	46	194	11
3MK7	0.99	1.02	0.053	0.020	0.0012	0.018	85	40	196	23
M8	0.72	0.46	0.050	0.021	-0.0020	0.020	97	44	153	44

Doing the same, but now for the model output when using the Wave Celerity Method, gives the values as in Table 4. Compared to the original ellipse parameters in Table 2, the signal-to-noise ratio is weaker. However, when comparing the outcome of the WC method to the outcome of the STEP method, the tidal signal is more strongly present in the M2 tide as can be seen in the signal-to-noise ratios. However, for the other tidal constituents, this is not the case and the signal-to-noise ratios for the predictions of the STEP method are larger. Looking at the tidal ellipse parameters, it can be seen that, just as for the STEP method, the outcome after applying the WC method differs quite a lot from the outcome of the original harmonic analysis, but for the M2 tide the size of the axis is close. One cause of this can be the overestimation of the amplitude for the eastward velocities after applying the harmonic analysis, as can be seen in Figures 22 and 23. Another cause can be the quality of the data influencing the outcome of the original accuracy of the parameters of the harmonic analysis.

Table 4: Mean variables for applying harmonic analysis for each of the grid cells after applying the WC method.

Tide	Signal-to-noise ratio		Major [m/s]		Minor [m/s]		Inclination [°]		Phase [°]	
	Mean	Std	Mean	Std	Mean	Std	Mean	Std	Mean	Std
K1	0.043	0.10	0.18	0.0068	0.0024	0.022	42	3	221	10
M2	3.07	0.78	0.58	0.014	0.024	0.087	45	2	161	10
M3	0.69	0.16	0.15	0.013	0.010	0.020	43	4	139	29
M4	0.49	0.22	0.030	0.0055	0.0062	0.010	48	15	261	29
2MK5	1.53	1.68	0.010	0.0059	-0.0031	0.0059	36	30	258	36
M6	1.29	0.82	0.027	0.0047	0.0013	0.0070	47	11	260	11
3MK7	1.94	1.14	0.031	0.0047	-0.020	0.0059	50	12	234	23
M8	0.67	0.31	0.0083	0.0017	-0.00091	0.0031	53	45	158	67

All in all, based on these results the ellipse parameters used to make the predictions of the model can not be verified for both methods and hence the assumption of using an average location for the harmonic analysis can not be supported However, this could be caused by several factors, such as the overestimation of the eastward velocity amplitude from the tidal ellipse and the quality of the data.

6.2 Comparison with Other Data Sources

To validate the output of the model, the output of the STEP and WC methods is compared to two other sources recording flow velocity data.

6.2.1 Dutch Coastal Shelf Model

For the comparison with the DCSM, multiple observation points for the middle of each grid cell over the entire model are assigned. Furthermore, inside the model domain there are two areas where a lot of measurements are made, as can be seen in Figure 3. For both of these areas, a 7x7 grid is applied to have comparative data at the areas with a lot of data. The observation points can be seen in Figure 41.

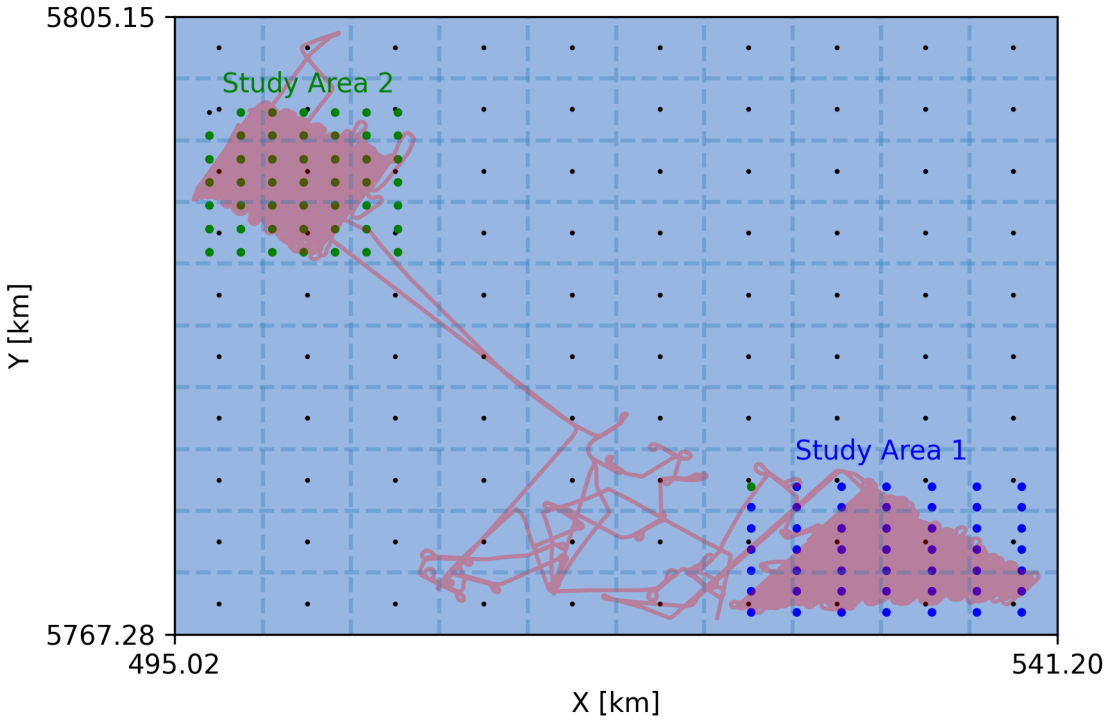

Figure 41: Locations of all observation points used for the DCSM in this study. The black points show the observation points over the entire model domain. The blue points show the observation points in Model Area 1 and the green points in Model Area 2.

The DCSM simulation is run for the entire month of May so that the warm-up period of the DCSM is over and the results between May 17 and May 21 can be used for comparison. In Figure 42, the result can be seen when comparing the output of the DCSM with the output of the STEP method applied for a depth-averaged water column. As can be seen, the DCSM output shows less variation in the predictions for the grid cell, while, as discussed before, the STEP method has a high variation in the predictions between grid cells. Furthermore, it can be seen that for the eastward velocities, the prediction of the DCSM is smaller than the prediction of the STEP method, showing again the overestimation of the eastward velocity amplitude. For the northward velocity, the DCSM predicted velocities are slightly higher, which can be caused by the fact that in the DCSM not only the same significant constituents as for the STEP method are taken into account but also other significant constituents, such as the S2 constituent.

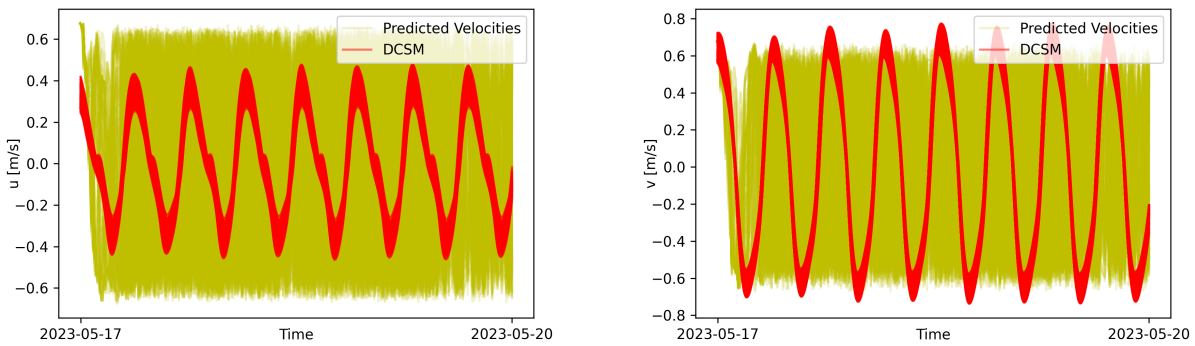

Figure 42: Comparison of the predicted eastward and northward velocity time series for each grid cell in the entire model domain, between the DCSM and the STEP method.

Comparing the outcome of the DCSM with the WC method, as shown in Figure 43, the predicted time series

are more similar than for the STEP method. The frequency, phase and variation in predicted velocities along the grid are similar. However, just as for the STEP method the eastward velocity is higher compared to the DCSM and the northward velocity is lower. The first can be explained by the overestimation of the eastward velocity amplitude from the tidal ellipse, while the second can be explained by the fact that the DCSM model considers more tidal constituents. Furthermore, the DCSM does not show peaks at the times the tide is changing direction, which is caused by a part of the tide turning clockwise for the WC method, instead of counterclockwise.

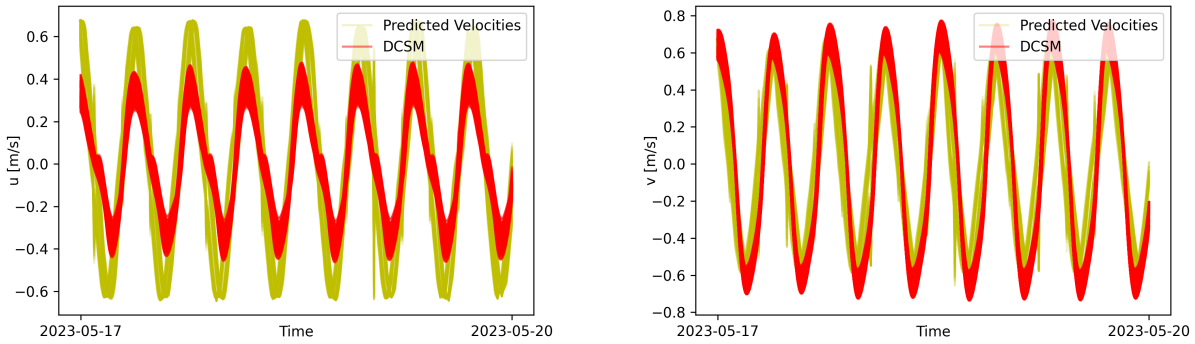

Figure 43: Comparison of the predicted eastward and northward velocity time series for each grid cell in the entire model domain, between the DCSM and the WC method.

To quantify the similarities and differences between the DCSM and the STEP or WC method, the cross-correlation and RMSD are calculated. For both, a distinction is made between the cross-correlation for the whole model area and the two areas with a lot of measurements. This will indicate whether the model performance is better in the areas with more data. The results for the entire model domain are shown in Table 5. Here it can be seen that the cross-correlation for both the eastward and northward velocities between the STEP method and the DCSM does not show much correlation, while for the WC method and the DCSM a high cross-correlation has been found, indicating that the phase and frequency of the outcomes of the WC method and the DCSM are similar. The RMSD score shows that there is less variation in the velocity magnitudes between the WC method and the DCSM compared to between the STEP method and the DCSM. Furthermore, while looking at the difference between the eastward and northward velocity it can be seen that the RMSD is smaller and there is a larger cross-correlation for the northward velocity .

Table 5: Cross-correlation (CC) and Root-Mean-Square Deviation (RMSD) between the model output and the DCSM, for both implemented methods, in the complete model domain.

Method	**Complete Model Domain**							
	Eastward Velocity				Northward Velocity			
	CC		RMSD		CC		RMSD	
	Mean	Std	Mean	Std	Mean	Std	Mean	Std
STEP	0.042	0.055	0.45	0.019	0.047	0.054	0.61	0.032
WC	0.91	0.035	0.23	0.028	0.94	0.045	0.16	0.048

Looking at the two study areas with more measurements, the cross-correlation and RMSD results are shown in Table 6 for Study Area 1 and in Table 7 for Study Area 2. As can be seen here the cross-correlation scores for the STEP method are similar when compared to the entire model domain, showing no correlation between the STEP method and the DCSM. Looking at the RMSD for the STEP method it can be seen that when more measurements are available the RMSD decreases and there is less difference between the STEP method and the DCSM. Looking at the results for the WC method it can be seen that there is much less correlation between the WC method and the DCSM compared to the entire model domain. This could be caused by the overestimation of the eastward velocity, causing a phase difference compared to the measurements. Looking at the RMSD for the WC method in those study areas, it can again be seen that the difference in velocity magnitudes is much smaller in the area where more measurements are available.

Table 6: Cross-correlation (CC) and Root-Mean-Square Deviation (RMSD) between the model output and the DCSM, for both implemented methods, in Study Area 1.

Method	**Study Area 1**							
	Eastward Velocity				Northward Velocity			
	CC		RMSD—		CC		RMSD	
	Mean	Std	Mean	Std	Mean	Std	Mean	Std
STEP	0.033	0.039	0.018	0.08	0.039	0.056	0.026	0.126
WC	0.33	0.0095	0.019	0.095	0.25	0.0042	0.029	0.14

Table 7: Cross-correlation (CC) and Root-Mean-Square Deviation (RMSD) between the model output and the DCSM, for both implemented methods, in Study Area 2.

Method	**Study Area 2**							
	Eastward Velocity				Northward Velocity			
	CC		RMSD		CC		RMSD	
	Mean	Std	Mean	Std	Mean	Std	Mean	Std
STEP	-0.051	0.041	0.014	0.082	0.0044	0.055	0.019	0.10
WC	0.31	0.0068	0.016	0.093	0.32	0.0019	0.019	0.11

In summary, this validation shows that while the STEP method has similar results for the velocity magnitudes, the phase and frequency of the predicted velocities differ significantly from the DCSM method, resulting in a low cross-correlation score and a high RMSD. For the WC method, the velocity magnitudes are similar, but also the phase and frequency are similar and only small differences are present between the WC method and the DCSM. This results in a high cross-correlation and a lower RMSD score for the WC method.

6.2.2 Buoy data

For the buoy data, the model results are compared with the buoy near IJmuiden, see Figure 3. The buoy measures the surface flow velocity and direction at that specific location in time steps of 10 minutes. To compare this to the model results, the model output for the uppermost layer of the water column of the measurements needs to be compared. Since the model currently does not contain all processes affecting the flow velocities, it is only interesting to compare the tidal flow velocities with the buoy. To get only the tidal velocities from the buoy measurements, harmonic analysis is applied to the buoy data, the output of which can be seen in Appendix A.3. From this harmonic analysis, only the M8 tide can be extracted from the buoy measurements, while the most important M2 constituent is not included.

Figure 44 shows that using the STEP method to get a prediction at the buoy location results in large differences between the buoy measurements and the predictions. The STEP method predictions show much more variation in magnitude, but also the phase and frequency of the output and tidal velocities from the buoy are different. This can be seen for both the eastward and northward velocity. The buoy measurements shows that a large difference is present with the output of the STEP model, but the magnitudes of the velocities are more similar.

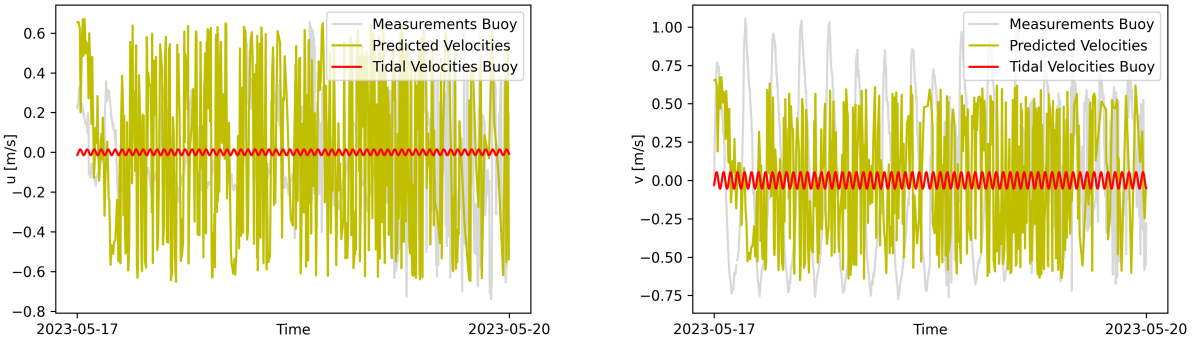

Figure 44: Comparison of the predicted eastward and northward velocity time series for each grid cell in the entire model domain, between the buoy measurements, tidal velocities extracted from the buoy measurements and the STEP method.

For the WC method, as shown in Figure 45, also large differences between the tidal signal extracted from the buoy measurements are present. The magnitude of the output of the WC method is much larger than the magnitude of the tidal velocities of the buoy. The magnitude of the buoy measurements are more similar but also show large differences. Furthermore, in the first half of the buoy measurements, some periodic behaviour can be observed, which has approximately the same frequency as the output of the WC method. However, the phase of the WC method output differs from that of the buoy measurements

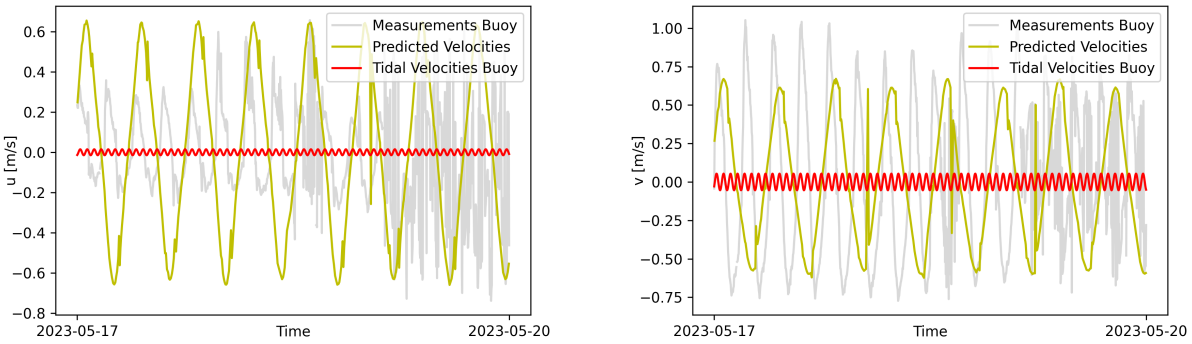

Figure 45: Comparison of the predicted eastward and northward velocity time series for each grid cell in the entire model domain, between the buoy measurements, tidal velocities extracted from the buoy measurements and the WC method.

To quantify the differences between the STEP method and the buoy and the WC method and the buoy, the cross-correlation and RMSD is calculated, shown in Table 8. This shows that for both the STEP and WC methods no significant cross-correlation is present for the northward and eastward velocity, caused by the differences in phase and frequency with respect to the tidal velocities of the buoy. Also, a large RMSD value is present for both methods and both the northward and eastward velocity, caused by the large difference in magnitude with respect to the tidal velocities of the buoy.

Table 8: Cross-correlation (CC) and Root-Mean-Square Deviation (RMSD) between the model output and the tidal velocities of the buoy near IJmuiden, for both implemented methods.

Method	Eastward Velocity		Northward Velocity	
	CC	RMSD	CC	RMSD
STEP	0.067	0.538	-0.10	0.542
WC	-0.055	0.540	-0.12	0.542

Comparing the buoy measurements, shown in Figure 46, to the output of the DCSM, the same results can be seen, a large difference in velocities magnitudes, phase and frequency compared to the measurements and tidal components for both the northward and eastward velocities.

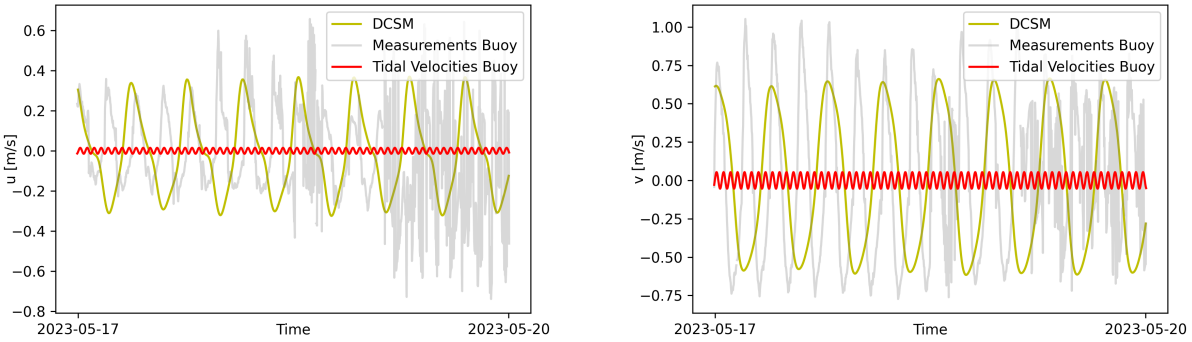

Figure 46: Comparison of the predicted eastward and northward velocity time series for each grid cell in the entire model domain, between the buoy measurements, tidal velocities extracted from the buoy measurements and the DCSM.

The differences with the buoy measurements can explained by three factors. First of all, the output of the tidal velocities only gives the M8 tides, while the most important tidal constituent, the M2 tide is not included. The STEP and WC methods both make predictions using more tidal constituents. Furthermore, the buoy measurements are surface flow measurements, while the DVL measurements only go as high as a water depth of -6 m. Lastly, the distance between the model domain and the location of the buoy is large. This means that along this distance many factors influence the flow velocities, causing the model predictions to differ from the buoy measurements. All in all, these issues need to be overcome to be able to accurately validate the output of both methods by making use of buoy measurements.

7 Discussion

The goal of this study was to develop a semi-empirical model based on the provided ship-based DVL measurements. This has the potential to overcome the low spatial resolution of buoy measurements, while also having a higher accuracy compared to the DCSM. To do this, first, the tidal components have been extracted using harmonic analysis. The research by Sheehan et al. (2018) showed that ship-based DVL measurements have an accuracy within ±0.4 cm/s, whiich is a high accuracy. Using DVL measurements in a harmonic analysis, gives the output shown in Table 9 in Appendix A.2. Here, it can be seen that the error margin for the major and minor axis of the tidal ellipse parameters is of the same order of magnitude and always within ±2 cm/s as desired for flow velocity predictions by hydrodynamic models in coastal shelf seas (Williams and Esteves, 2017). However, looking at the error for the inclination and phase of the tidal constituents, a large error margin exists, especially for the constituents with a low signal-to-noise ratio. This will have a large effect on the flow velocities, since a difference in phase has a large influence on the magnitude of the flow velocity vector, while a difference in the inclination will affect the direction of the flow and hence the eastward and northward flow velocity measurements. Hence, the accuracy of the tidal velocities predicted by the harmonic analysis in this research can be improved by reducing the errors in the tidal analysis and as shown by de Vreeze (2020), using ship-based DVL measurements it is possible to accurately estimate the tidal ellipse with a RMSD of 1-3 cm/s. Since the error in the output of the STEP and WC methods is not known, no judgement can be made on whether this method has a higher accuracy when predicting flow velocities compared to the DCSM. However, if better data was available to use in the STEP and WC methods and a good validation data set is available, the quality of the predictions for both methods can be assessed, to see if it is an improvement on the accuracy of the DCSM method, which overestimates the model up to 6-7 cm/s (Zijl et al., 2018) and whether the methods have the potential to be within the desired margin of ±2 cm/s. Hence, to be able to decide whether the methods developed in this study are available a higher quality data set is needed and a better validation data set is needed to compare the predictions.

The output of the harmonic analysis can be improved if higher quality data is available. This can be achieved

by changing the way the measurements are made. The most important improvement is to make sure that the internal clock of the DVL and the software on the ship are synchronised so that the heading pitch and roll corrections are applied at the right moment. Since this is currently not the case, the moments where the boat is turning are filtered out, therefore synchronising the clocks would result in more data. Moreover, providing more data measured by the DVL can help with the choices made in the pre-processing of the data. If the measured vertical velocity is provided a more substantiated choice can be made to filter out the effect of the ship. Furthermore, having more frequent measurements, instead of once every 10 seconds, decreases the standard deviation in the measurements (Huitema, personal communication, June 1, 2023). Hence, to get high-quality flow velocity data the DVL should be set-up in the right way.

Looking at the output of the STEP method, it can be seen that the calculation of the spatial phase difference is too large. This could be caused by the way the averaging of the different spatial phase differences is calculated for each grid cell. First of all, whether the temporal and spatial phase differences are positive or negative is not taken into account in the current averaging method. This can mean that one grid cell has a negative spatial phase difference because the measurements are made at an earlier moment than inside the current grid cell, while the grid cell next to it can have a positive spatial phase difference, because the measurements are made at a later moment. To deal with this, the sign of the temporal phase difference should be taken into account. Next to this, applying a weighted average based on the spatial and temporal distance to this grid cell would make sure that measurements made closer, in both space and time, have more effect on the prediction. This is beneficial since it is likely that measurements made farther away or at a later moment have less correlation with the current measurements.

The validation of the STEP method with the DCSM showed that the frequency of the predicted tidal wave in the STEP method and hence the spatial phase difference is too large. The validation of the WC method with the DCSM showed a high cross-correlation and a low RMSD score, indicating a high similarity between the results of both models. Since the DCSM is widely tested and used, these results are likely to be qualitatively correct. Looking at the results of the WC method, the need to have high-resolution flow velocity measurements can be seen. In the model domain can be seen that over a distance of 40 km a phase difference of 40° can be observed, which can lead to significant differences in flow velocities. This means that, when using buoy measurements as hydrodynamic data, the accuracy of the input data significantly decreases when making predictions only a small distance away. Furthermore, since the closest buoy with flow velocity measurements to the study area was the buoy near IJmuiden, which is around 80 km away, a phase difference of around 90° would be present, which can mean the difference between high tide and the tides changing direction. Hence, large differences would be visible if the flow velocity data of this buoy is used as hydrodynamical input data for this model.

Validating the output of the STEP and WC methods based on the tidal velocities obtained from buoy near IJmuiden was not possible because of the lack of the most important M2 constituent. However, this comparison does highlight another shortcoming of the buoy measurements. Looking at Figures 50 and 51 in Appendix A.3, shows that at the end of the time series, a lot more variation in the eastward and northward velocities is present. This makes it harder to extract the tidal signal from this data set. A reason for this is that near the water surface, a lot of turbulence is present, caused by breaking waves, precipitation, ships passing by and thermal convection (Thorpe, 1995). Since the buoy is placed at the water surface, the measurements made by the buoys can be affected, as was the case for this buoy, and therefore make the output of the harmonic analysis less useful. Since a study by Sheehan et al. (2018) showed that this is possible to get an accuracy within ±0.4 cm/s, using ship-based DVL measurements, this method can overcome this problem.

An advantage of the STEP and WC methods compared to the DCSM is that the grid resolution and the amount of depth layers considered can be freely changed. In the DCSM the grid is fixed, but for both developed methods, the grid can be easily adjusted. This means a coarser grid can be defined if low-resolution data is needed and hence the computation time can be decreased, but if high-resolution data is needed the cell size can also be adjusted. The same holds for the depth-layers. The DCSM can be run as a 3D model or as a 2DH model, but for the developed methods the user can choose how many depth layers are considered and where the split point of these layers are. The only limitation is that a depth layer must have a height of at least 2 m since the measurements are made with depth increments of 2 m. Also, due to the turbulence caused by the ship, this method does not provide flow velocities near the surface.

A disadvantage of the ship-based DVL measurements is that there is no prediction of the near-bed velocities, caused by the side lobes of the DVL. This effect was also visible in the velocity profiles, where close to the seabed the velocity profile was significantly different. Accurate near-bed velocities are needed to get accurate

predictions when using morphodynamic models. This can be resolved by estimating the near-bed velocities based on the velocity in the lowest depth layer, as done by morphodynamic models using ship-based DVL measurements as input data (Zhou et al., 2022). However, this increases the uncertainty of the near-bed velocities.

There are several steps that can be taken to improve the output of the developed methods. For the harmonic analysis in this study, an input time series of 4 days is used. However, many important tidal constituents, such as the spring-neap cycle, have longer cycles and are therefore not included in the analysis. Hence, to make sure the most important tidal constituents are included in the analysis, the measured velocity time series should at least be 30 days long and preferably longer to include even more tidal constituents (Stephenson, 2016). The DCSM uses 39 tidal constituents and the STEP method and WC method 6, causing differences in the predicted velocities. To get a more accurate comparison with the DCSM more tidal constituents have to be included in the STEP and WC method.

The harmonic analysis deals with the spatial distribution of the measurements by assuming that the measurements are made at one location and then applying the harmonic analysis. However, if the measurements are made far apart it is more likely that this assumption is incorrect. A solution to this would be to split the measurements into multiple zones, based on their location and then for each zone apply the harmonic analysis, provided enough data is available to ensure enough tidal constituents can be extracted, In this research this has not been done, because only 4 days of data was available and splitting this data would result in even less tidal constituents considered in the harmonic analysis.

Another improvement that can be made is in the validation of the model output. In this research, a comparison is made with a buoy that is far outside the model domain. Ideally, a buoy should be present within the model domain so that the correlation between the two locations of the buoy and the model output is higher. Besides this, the buoy used only measures the surface flow velocity. Due to the set-up of the DVL on the ship, this has not been measured by the DVL. Hence, a buoy measuring velocities at different depths would be the most useful for comparison. Another way this can be done is by placing a fixed ADCP inside the model domain that makes measurements at the same moments as the DVL.

Another way to validate the data is to split a part of the data into a validation data set. Making predictions based on the rest of the data at the times and locations of the validation measurements would then show whether the two methods are able to make accurate predictions. Because of the limited amount of data available in this research, this has not been done, but if more data is available this would be interesting to test.

A possible issue lies with the way the tidal ellipse parameters are validated. The outcome of the harmonic analysis performed by using `T_Tide`, is checked by again performing the harmonic analysis using `T_Tide`. This means that the outcome of a model is checked by the same model. While this does say something about the tidal propagation model results, some of the information of the tidal signal will be lost when performing the harmonic analysis again, leading to different tidal ellipse parameters. Hence, to have a complete validation of the tidal ellipse parameters, measurements of the tidal ellipse should be available for a grid cell.

In case the model output gets improved, many further steps can be taken to increase the performance of the model. Now, arbitrary choices have been made about the grid and the amount of depth layers in the model. Research into the stability of the model for different grid sizes and models would indicate how many measurements are needed per grid cell and depth layer for the model to yield accurate results. Furthermore, now a rectangular grid is considered, but a triangular grid could be implemented when a more flexible grid is desired, where the resolution of the grid can change between each of the grid cells. It is also possible to combine both types of grid.

Another interesting area of further research is to check the performance of the model based on the size of the model domain and specifically for the grid cells having no measurements at all. This can give an indication of how far the model output can be extrapolated. To do this, another data source needs to be available to check the model at such locations, such as fixed ADCP or buoys making velocity measurements. At the moment it can be seen that within the model domain, the velocities predicted by the WC method are similar to the velocities in the DCSM model, hence within the model domain the performance of WC method is good. For the STEP method, it can be seen that the current performance within the model domain is not good. Furthermore, since the buoy near IJmuiden only measures surface flow velocities and only the M8 constituent could be extracted from these measurements, meaning that comparing the STEP method and WC method and the buoy measurement gives no information about the performance of the STEP and WC

method for this distance.

Finally, the developed model is not a complete hydrodynamic model but contains only the tidal signal. However, many more factors affect the flow velocity in the North Sea, such as wind, waves (Thorpe, 1995), inflowing rivers (e.g. De Boer et al., 2006), the coast, human activities, and many more. Hence, the developed model is currently not meant to be used to make predictions. For this, further research has to be conducted on how to add these factors to the model.

8 Conclusion

This report shows the first steps taken to make a hydrodynamic model based on ship-based DVL or ADCP measurements. To do this the main research questions was:

In what way can a semi-empirical model be developed to express flow velocities and directions in a marine environment, based on ship-based DVL measurements?

To answer this, the three sub-research questions were answered:

How can the DVL data be used as input for a hydrodynamic semi-empirical model?
The DVL data received first needed to be pre-processed. The steps taken in the pre-processing include leaving out the top layer and bottom 10% of the water column to deal with the effects of the ship and side lobes on the measurements respectively. Besides this, the time logging difference between the DVL and the ship has been explained to show the need to synchronize the clock of the DVL and the software of the ship. After this, the outliers of the velocity magnitude, eastward and northward velocities are filtered based on the standard deviation of the measurements. Lastly, the model is divided into different depth layers by looking at the different velocity profiles.

What semi-empirical model can be developed for flow velocities and directions in a marine environment?
To develop a model, first the tidal velocities have been extracted from the data. This is done by performing a harmonic analysis of the pre-processed data. This showed that for the top part of the water column, the significant tidal constituents are the M2, M3, M4, 2MK5, M6 and M8 tides and for the bottom part of the water column, the significant tidal constituents are the M2 and 2MK5 tides. In the harmonic analysis, the amplitude of the northward velocity is correctly estimated, but for the eastward velocity, the amplitude is twice as large when compared to the measurements. Based on these tidal signals, the propagation of the tides is predicted. To deal with the spatial and temporal differences in the DVL measurements two methods have been developed. The STEP method estimates the spatial phase difference based on the temporal phase differences in all grid cells, calculated from other measurements. The output of this model showed that this method significantly overestimates the spatial phase difference, causing differences of up to 20000°, caused by not taking the sign of the temporal difference into account when averaging . For the WC method, which is based on the wave celerity in the model domain, the output is more realistic, showing a spatial phase difference in the model domain of at most 40°.

What differences exist with other flow velocity data sources?
Comparing the output of the STEP method and WC method with the output of the DCSM shows that the frequency and phase of the STEP method differs a lot, leading to a low cross-correlation score of around 0 and a high RMSD score of 0.45 m/s up to 0.61 m/s over the entire model domain. For the WC method, the phase and frequency were much more similar, leading to a high cross-correlation of around 0.91 and a low RMSD of around 0.2 m/s. However, for both methods, the eastward flow velocities are slightly higher and the northward slightly lower compared to the DCSM. Also, the DCSM includes 39 tidal constituents in the output, while the STEP and WC methods could only include at most 6 tidal constituents. Comparing the STEP and WC methods with the buoy measurements near IJmuiden did not show any concrete results, since the buoy measured only the surface flow velocities and only the M8 tidal constituent could be extracted, while the STEP and WC method can not predict surface flow velocities and includes more tidal constituents. Also, the buoy was far away from the study area, making the correlation between the measurements lower.

Two methods have been implemented, with potential advantages compared to existing data sources. First of all, this model would take the spatial variation of the flow in a marine environment into account, which is an improvement over buoy measurements, and the model is based on measurements with a high accuracy, which can improve the quality of the predictions made compared to coastal shelf models such as the DCSM. Furthermore, this model has a high flexibility in grid spacing and in the depth layers included in the model. This means that the output of the model can be easily adjusted to the desired needs. The WC method showed promising results by providing a similar prediction as the DCSM methods. On the other hand, the STEP

method overestimates the spatial phase difference and this problem should be solved before this method can be developed further. For both models, before they can be used, more validation has to take place on the model results, after which the methods can be extended by including more physical processes.

9 Recommendations

If someone wants to continue with this project, these are the main recommendations when making new ship-based DVL measurements

9.1 Quality of the Data

- Make sure that the internal clock of the DVL or ADCP is synchronized with the software on the ship. This makes sure that the corrections of the pitch and roll and the heading are applied at the correct moment.
- Make measurements for a period of at least 30 days. This includes the most important tidal constituents in the harmonic analysis
- Also include the vertical velocity measurements in the data set. In this way, more substantiated choices about the steps taken can be made during the pre-processing of the data, such as the amount of depth layers to filter out.
- Increase the sampling frequency of the DVL or ADCP. This leads to more measurements, leading to a decrease in the standard deviation of the measurements.
- Make measurements in a model domain with a buoy measuring velocities at different water depths or place a fixed ADCP somewhere in the model domain to make these measurements. In this way, a validation of the model can be improved since a nearby data source can be used to compare with the measurements.

9.2 Model Development

Furthermore, here are some recommendations to improve the model.

- For the STEP method, include weighted averaging in the model. This makes sure that the spatially and temporally close measurements have more influence on the predictions since these are likely to have a high correlation.
- If enough data is available, split the data set into multiple zones and perform the harmonic analysis for each of these zones. In this way, the effect of assuming that the measurements are made at one location is decreased when performing the harmonic analysis, since this is now done at multiple locations.
- If enough data is available, split the data set into a testing set and a validation set. In this way, the model predictions can be validated on the data itself and no other data sources are needed.
- Test the accuracy of the model based on different distances for which the predictions are made. This will give an indication of the spatial resolution needed to ensure that the measurements will remain accurate and how far the model predictions can be extrapolated.
- Before including other physical processes, validate the output of the used method. Otherwise, it will not be clear whether possible errors in predictions are caused by the tidal component or the added physical process.

References

Bourke, P. (1996). Cross correlation, autocorrelation, 2D pattern identification. https://www.researchgate.net/publication/245817141_Cross_correlation_autocorrelation_2d_pattern_identification

De Boer, G. J., Pietrzak, J. D., & Winterwerp, J. C. (2006). On the vertical structure of the Rhine region of freshwater influence. *Ocean dynamics*, *56*, 198–216. https://doi.org/10.1007/s10236-005-0042-1

de Vreeze, S. (2020). Observing ocean currents on the Scottish Continental Shelf using. http://essay.utwente.nl/83200/

Doodson, A. T. (1921). The harmonic development of the tide-generating potential. *Proceedings of the Royal Society of London. Series A, Containing Papers of a Mathematical and Physical Character*, *100*(704), 305–329. https://doi.org/10.1098/rspa.1921.0088

Dyer, K. R., & Huntley, D. A. (1999). The origin, classification and modelling of sand banks and ridges. *Continental Shelf Research*, *19*(10), 1285–1330. https://doi.org/https://doi.org/10.1016/S0278-4343(99)00028-X

Elias, E. (2017). Kustgenese 2.0; available measurments and bathymetric data at Ameland inlet, The Netherlands. https://publications.deltares.nl/1220339_007b.pdf

Fang, G., & Ichiye, T. (1983). On the vertical structure of tidal currents in a homogeneous sea. *Geophysical Journal International*, *73*(1), 65–82. https://doi.org/10.1111/j.1365-246X.1983.tb03807.x

Fong, D. A., & Jones, N. L. (2006). Evaluation of AUV-based ADCP measurements. *Limnology and Oceanography: methods*, *4*(3), 58–67. https://doi.org/10.4319/lom.2006.4.58

Fong, D. A., & Monismith, S. G. (2004). Evaluation of the accuracy of a ship-mounted, bottom-tracking ADCP in a near-shore coastal flow. *Journal of atmospheric and oceanic technology*, *21*(7), 1121–1128. https://doi.org/10.1175/1520-0426(2004)021⟨1121:EOTAOA⟩2.0.CO;2

Foreman, M. G. G., & Henry, R. F. (1989). The harmonic analysis of tidal model time series. *Advances in water resources*, *12*(3), 109–120. https://doi.org/10.1016/0309-1708(89)90017-1

Games, K. P., & Gordon, D. I. (2014). Study of sand wave migration over five years as observed in two windfarm development areas, and the implications for building on moving substrates in the North Sea. *Earth and Environmental Science Transactions of the Royal Society of Edinburgh*, *105*(4), 241–249. https://doi.org/10.1017/S1755691015000110

González-Castro, J. A., & Muste, M. (2007). Framework for estimating uncertainty of ADCP measurements from a moving boat by standardized uncertainty analysis. *Journal of Hydraulic Engineering*, *133*(12), 1390–1410. https://doi.org/10.1061/(ASCE)0733-9429(2007)133:12(1390)

Guerra, M., & Thomson, J. (2017). Turbulence measurements from five-beam acoustic Doppler current profilers. *Journal of Atmospheric and Oceanic Technology*, *34*(6), 1267–1284. https://doi.org/10.1175/JTECH-D-16-0148.1

Hodson, T. O. (2022). Root-mean-square error (RMSE) or mean absolute error (MAE): When to use them or not. *Geoscientific Model Development*, *15*(14), 5481–5487. https://doi.org/10.5194/gmd-15-5481-2022

Horstman, E. M., Balke, T., Bouma, T. J., Dohmen-Janssen, C. M., & Hulscher, S. J. M. H. (2011). Optimizing methods to measure hydrodynamics in coastal wetlands: Evaluating the use and positioning of ADV, ADCP and HR-ADCP. *Coastal Engineering Proceedings*, (32), 51–51. https://doi.org/10.9753/icce.v32.waves.51

Howarth, M., & Proctor, R. (1992). Ship ADCP measurements and tidal models of the North Sea. *Continental Shelf Research*, *12*(5-6), 601–623. https://doi.org/10.1016/0278-4343(92)90022-C

Huitema, H. (June 1, 2023). Personal communication.

Iglesias, I., Bio, A., Melo, W., Avilez-Valente, P., Pinho, J., Cruz, M., Gomes, A., Vieira, J., Bastos, L., & Veloso-Gomes, F. (2022). Hydrodynamic model ensembles for climate change projections in estuarine regions. *Water*, *14*(12), 1966. https://doi.org/10.3390/w14121966

Kawanisi, K. (2004). Structure of turbulent flow in a shallow tidal estuary. *Journal of Hydraulic engineering*, *130*(4), 360–370. https://doi.org/10.1061/(ASCE)0733-9429(2004)130:4(360)

Li, G., Xu, K., Xue, Z. G., Liu, H., & Bentley, S. J. (2021). Hydrodynamics and sediment dynamics in Barataria Bay, Louisiana, USA. *Estuarine, Coastal and Shelf Science*, *249*, 107090. https://doi.org/10.1016/j.ecss.2020.107090

Maas, L. R. M., & Van Haren, J. J. M. (1987). Observations on the vertical structure of tidal and inertial currents in the central North Sea. *Journal of Marine Research*, *45*(2), 293–318. https://doi.org/10.1016/0077-7579(90)90030-K

Nortek. (2023a). DVL Compact -6000 m - Doppler Velocity Log [[Accessed 24-Jul-2023]]. https://www.nortekgroup.com/products/compact-dvl500-4000

Nortek. (2023b). Signature 500 - Current Profiler [[Accessed 24-Jul-2023]]. https://www.nortekgroup.com/products/compact-dvl500-4000

Nortek. (2023c). Understanding ADCPs: A guide to measuring currents, waves turbulence — nortekgroup.com [[Accessed 16-08-2023]]. https://www.nortekgroup.com/knowledge-center/wiki/guide-to-understanding-adcps

Overes, P. H. P., Borsje, B. W., Luijendijk, A. P., & Hulscher, S. (2023). Exploring the main drivers of sand wave dynamics. *7th Marine and River Dune Dynamics, MARID 2023*, 231–237. https://ris.utwente.nl/ws/files/303089037/overes.pdf

Pandian, P. K., Emmanuel, O., Ruscoe, J., Side, J., Harris, R., Kerr, S., & Bullen, C. (2010). An overview of recent technologies on wave and current measurement in coastal and marine applications. *Journal of Oceanography and Marine Science*, *1*(1), 1–10. https://doi.org/10.5897/JOMS.9000002

Pawlowicz, R., Beardsley, B., & Lentz, S. (2002). Classical tidal harmonic analysis including error estimates in MATLAB using T_TIDE. *Computers & geosciences*, *28*(8), 929–937. https://doi.org/10.1016/S0098-3004(02)00013-4

Persson, A. (2005). The Coriolis Effect. *History of Meteorology*, *2*, 1–24. https://journal.meteohistory.org/index.php/hom/article/view/30

Plecha, S., Silva, P. A., Oliveira, A., & Dias, J. M. (2012). Establishing the wave climate influence on the morphodynamics of a coastal lagoon inlet. *Ocean Dynamics*, *62*(5), 799–814. https://doi.org/10.1007/s10236-012-0530-z

Ribotti, A., Borghini, M., Satta, A., & Magni, P. (2019). Ship-Mounted Acoustic Doppler Current Profiler (ADCP): Characteristics and Field Applications to Measure Coastal Hydrodynamics. https://doi.org/10.1002/9781119300762.wsts0084

Rijkswaterstaat. (2023). Waterinfo Rijkswaterstaat [[Accessed 25-Sep-2023]]. https://www.nortekgroup.com/products/compact-dvl500-4000

Schrijvershof, R., Brakenhoff, L., & Grasmeijer, B. (2019). Hydrodynamics and bedforms on the Dutch lower shoreface. https://publications.deltares.nl/1220339_007.pdf

Sheehan, P. M., Berx, B., Gallego, A., Hall, R. A., Heywood, K. J., Hughes, S. L., & Queste, B. Y. (2018). Shelf sea tidal currents and mixing fronts determined from ocean glider observations. *Ocean Science*, *14*(2), 225–236. https://doi.org/10.5194/os-14-225-2018

Singh, S. K., Debnath, K., & Mazumder, B. S. (2016). Spatially-averaged turbulent flow over cubical roughness in wave-current co-existing environment. *Coastal Engineering*, *114*, 77–85. https://doi.org/10.1016/j.coastaleng.2016.04.013

Stephenson, A. G. (2016). Harmonic analysis of tides using TideHarmonics. https://CRAN.R-project.org/package=TideHarmonics

The Netherlands Hydrographic Service. (2023). Bathymetry Data.

Thorpe, S. (1995). Dynamical processes of transfer at the sea surface. *Progress in Oceanography*, *35*(4), 315–352. https://doi.org/10.1016/0079-6611(95)80002-B

Van Gils, A. (2014). Validation of X-band radar derived hydrodynamic phenomena. https://repository.tudelft.nl/islandora/object/uuid%3A56bddc1f-493f-47a7-b4c5-92583a6243aa

Van Prooijen, B. C., Tissier, M. F. S., De Wit, F. P., Pearson, S. G., Brakenhoff, L. B., Van Maarseveen, M. C. G., Van Der Vegt, M., Mol, J., Kok, F., & Holzhauer, H. (2020). Measurements of hydrodynamics, sediment, morphology and benthos on Ameland ebb-tidal delta and lower shoreface. *Earth system science data*, *12*(4), 2775–2786. https://doi.org/10.5194/essd-12-2775-2020

Walters, R. A. (1987). A model for tides and currents in the English Channel and southern North Sea. *Advances in water Resources*, *10*(3), 138–148. https://doi.org/10.1016/j.margeo.2006.10.001

Williams, J. J., & Esteves, L. S. (2017). Guidance on setup, calibration, and validation of hydrodynamic, wave, and sediment models for shelf seas and estuaries. *Advances in civil engineering*, *2017*. https://doi.org/10.1155/2017/5251902

Wilson, D., & Siegel, E. (2008). Evaluation of current and wave measurements from a coastal buoy. *OCEANS 2008*, 1–5. https://doi.org/https://doi.org/10.1109/OCEANS.2008.5152108

Xu, Z. (2000). Ellipse parameters conversion and vertical velocity profiles for tidal currents in MATLAB. *Bedford Institute of Oceanography, Dartmouth, Nova Scotia, Canada*, *20*. https://doi.org/10.13140/RG.2.1.2515.4000

Zhou, J., Wu, Z., Zhao, D., Guan, W., Cao, Z., & Wang, M. (2022). Effect of topographic background on sand wave migration on the eastern Taiwan Banks. *Geomorphology*, *398*, 108030. https://doi.org/10.1016/j.geomorph.2021.108030

Zijl, F., Groenenboom, J., Laan, S., & Zijlker, T. (2023). 3D DCSM FM: a sixth-generation model for the NW European Shelf. https://publications.deltares.nl/11208054_000_0010.pdf

Zijl, F., Veenstra, J., & Groenenboomr, J. (2018). The 3D Dutch Continental Shelf Model - Flexible Mesh (3D DCSMFM). https://www.deltares.nl/en/expertise/publicaties/3d-dutch-continental-shelf-model-flexible-mesh-3d-dcsmfm-setup-and-validation

A Appendix

A.1 Filtering Results

In Figures 47, 48 and 49, the results of the filtering process explained in Section 3.2.3 can be seen when using 3, 5 and 6 standard deviations respectively.

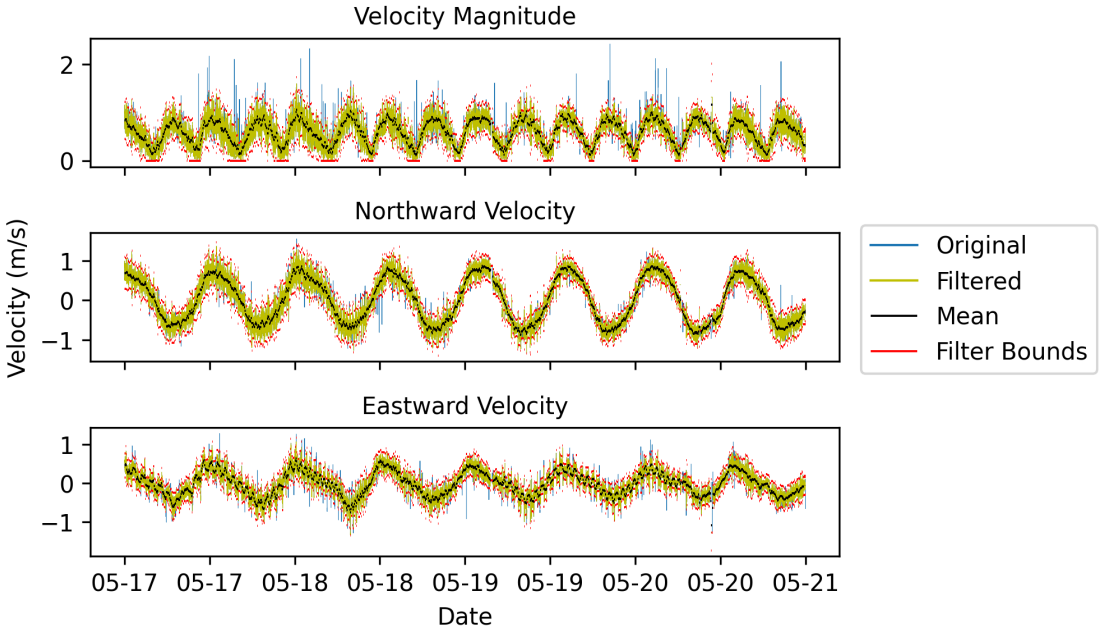

Figure 47: Filtering process for a complete time series based on 3 standard deviations of with respect to the mean velocity for overlapping batches of 10 minutes at a water depth of 7 meters.

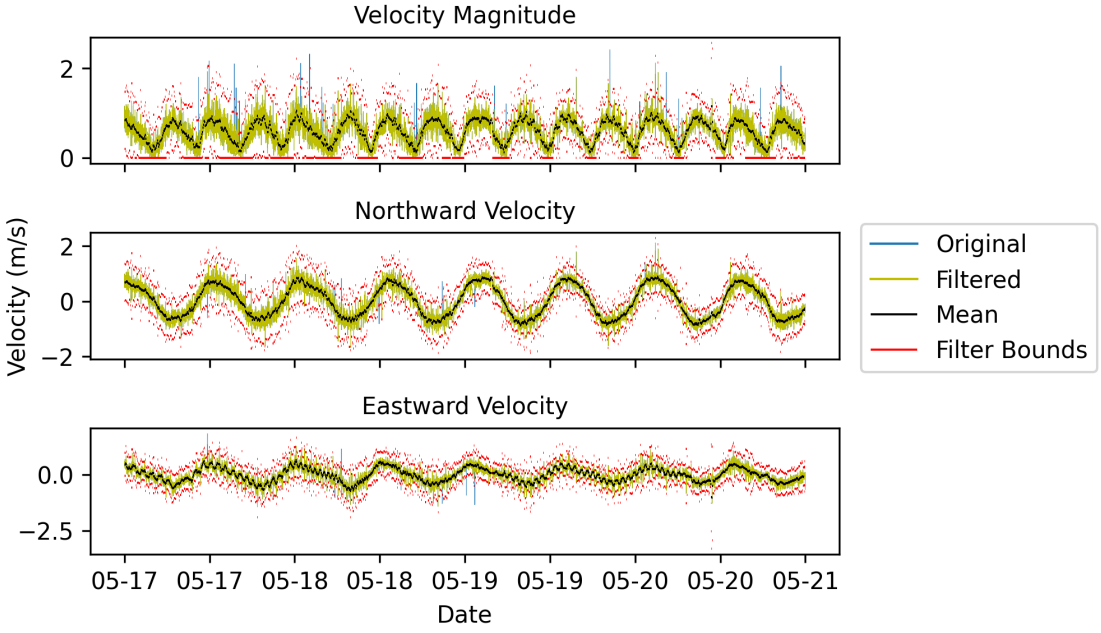

Figure 48: Filtering process for a complete time series based on 5 standard deviations of with respect to the mean velocity for overlapping batches of 10 minutes at a water depth of 7 meters.

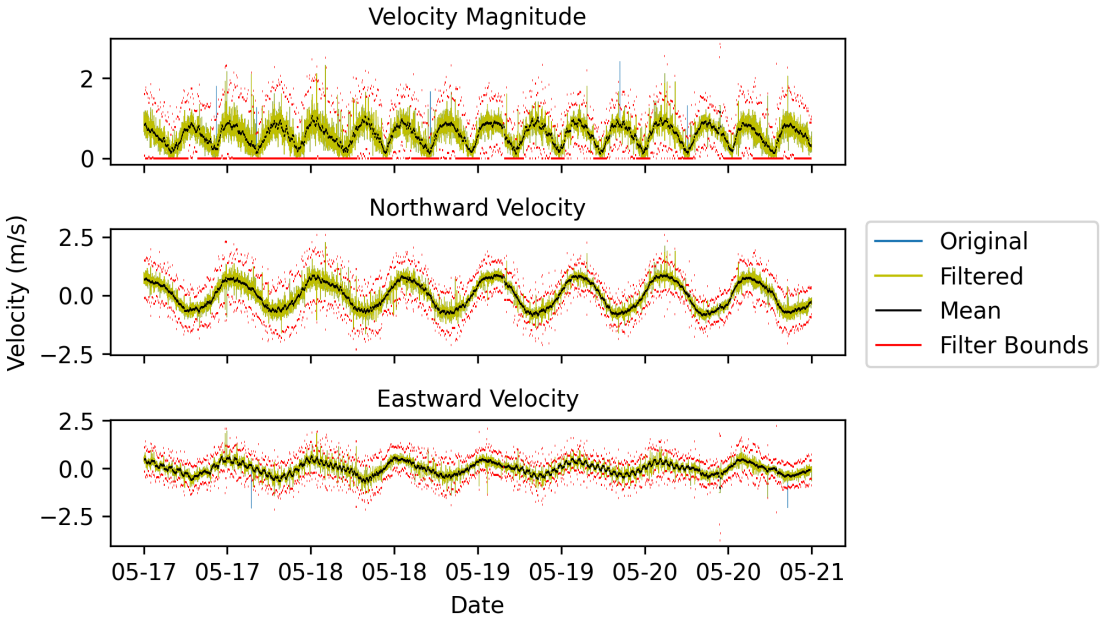

Figure 49: Filtering process for a complete time series based on 6 standard deviations of with respect to the mean velocity for overlapping batches of 10 minutes at a water depth of 7 meters.

A.2 Harmonic Analysis Output

In Tables 9 and 10 the complete output of the harmonic analysis performed in Section 5.1 is shown for the top part and the bottom part of the water column, using the split based on the velocity profiles explained in Section 3.3.

Table 9: Output of the Harmonic Analysis performed for the top part of the water column.

Tide	Frequency	Major Axis	Error Major Axis	Minor Axis	Error Minor Axis	Inclination	Error Inclination	Phase	Error Phase	Signal-to-Noise Ratio
K1	0.0417807	0.0408	0.053	-0.0105	0.038	74.94	53.16	42.19	110.43	0.59
M2	0.0805114	0.7437	0.063	0.0577	0.055	64.43	3.88	60.74	5.44	$1.4 \cdot 10^2$
M3	0.1207671	0.0305	0.013	0.0079	0.020	25.61	46.01	262.60	34.25	5.2
M4	0.1610228	0.0850	0.009	0.0104	0.019	4.48	15.56	23.46	6.15	95
2MK5	0.2028035	0.0175	0.008	-0.0001	0.006	157.50	23.76	343.54	30.43	4.8
M6	0.2415342	0.0610	0.005	-0.0081	0.005	78.76	12.31	53.14	3.15	$1.8 \cdot 10^2$
3MK7	0.2833149	0.0032	0.007	-0.0004	0.005	65.88	57.30	338.34	159.74	0.18
M8	0.3220456	0.0214	0.010	-0.0043	0.008	18.24	41.29	20.90	11.38	4.2

Table 10: Output of the Harmonic Analysis performed for the bottom part of the water column.

Tide	Frequency	Major Axis	Error Major Axis	Minor Axis	Error Minor Axis	Inclination	Error Inclination	Phase	Error Phase	Signal-to-Noise Ratio
K1	0.0417807	0.0184	0.077	-0.0010	0.055	88.02	44.26	54.22	187.60	0.057
M2	0.0805114	0.1821	0.113	0.0055	0.073	70.33	20.08	63.28	40.64	2.6
M3	0.1207671	0.0079	0.008	0.0021	0.005	18.43	38.24	267.38	81.93	1.1
M4	0.1610228	0.0160	0.013	-0.0079	0.013	3.16	86.38	6.75	73.33	1.5
2MK5	0.2028035	0.0189	0.013	0.0052	0.015	17.61	55.19	202.82	50.73	2.2
M6	0.2415342	0.0170	0.014	0.0028	0.022	103.01	122.28	22.29	70.89	1.4
3MK7	0.2833149	0.0046	0.010	0.0015	0.010	34.49	120.39	54.24	171.91	0.23
M8	0.3220456	0.0138	0.016	0.0041	0.015	166.03	73.89	100.32	98.71	0.73

A.3 Harmonic Analysis Buoy

Figures 50 and 51 show the input time series used in the harmonic analysis for the buoy data, which yields the tidal signal and residue signal for both the eastward and northward velocity, as used in Section 6.2.2

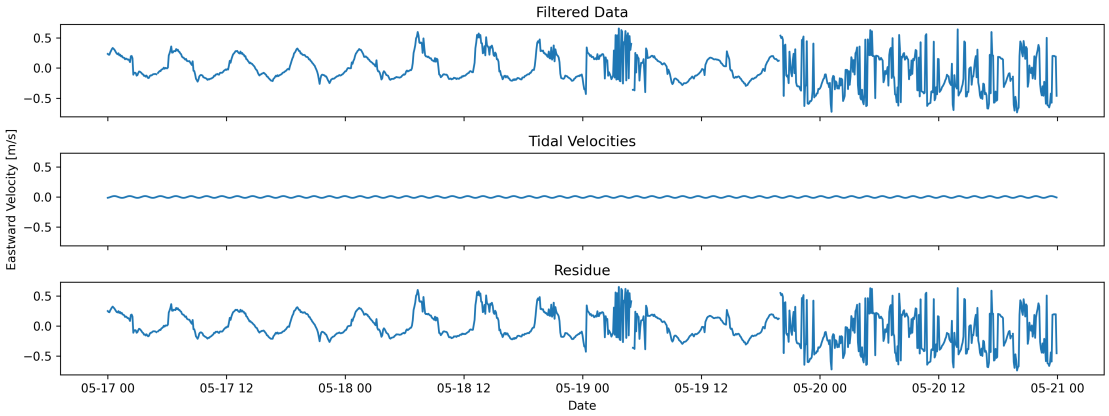

Figure 50: Input and output of the harmonic analysis for the northward velocities for the buoy near IJmuiden.

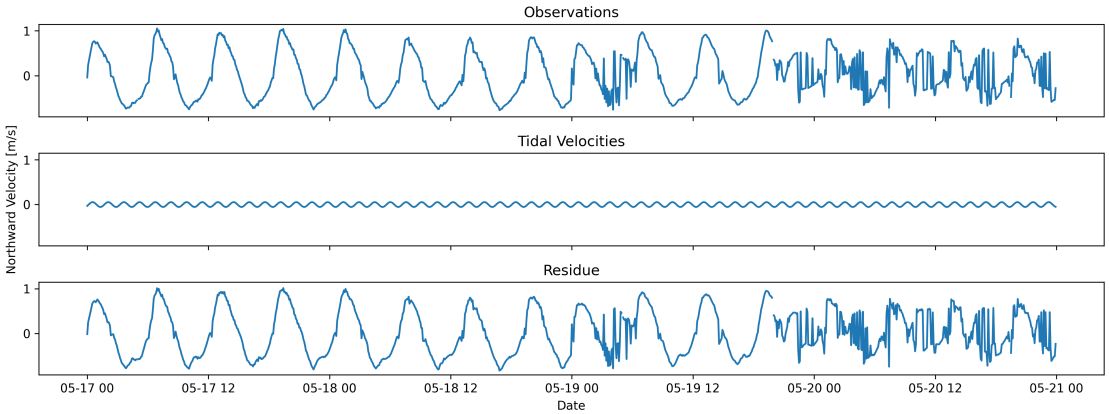

Figure 51: Input and output of the harmonic analysis for the eastward velocities for the buoy near IJmuiden.